JGR Space Physics

RESEARCH ARTICLE
10.1029/2019JA027102

# Low Frequency (f < 200 Hz) Polar Plasmaspheric Hiss: Coherent and Intense

**Bruce T. Tsurutani[1], Sang A. Park[2], Barbara J. Falkowski[3], Jacob Bortnik[4], Gurbax S. Lakhina[5], Abhijit Sen[6], Jolene S. Pickett[7], Rajkumar Hajra[8], Michell Parrot[9], and Pierre Henri[9]**

[1]Retired, Pasadena, CA, USA, [2]Electrical Engineering and Computer Sciences, University of California, Berkeley, CA, USA, [3]Glendale Community College, Glendale, CA, USA, [4]University of California, Los Angeles, Los Angeles, CA, USA, [5]Indian Institute of Geomagnetism, Navi Mumbai, India, [6]Institute for Plasma Research, Gandhinagar, India, [7]University of Iowa, Iowa, IA, USA, [8]Indian Institute of Technology Indore, Indore, India, [9]LPC2E, CNRS, Orléans, France

**Key Points:**
- Intense Low Frequency (~22 to 200 Hz) is found to be coherent at all local times. The waves are most intense in the noon sector
- Intense noon sector hiss is substorm dependent and solar wind pressure independent. A hypothesis of min. B pocket chorus origin is given
- LF hiss can be circularly, elliptically and linearly polarized. The majority of waves are elliptically polarized

**Correspondence to:**
B. T. Tsurutani,
bruce.tsurutani@gmail.com

**Citation:**
Tsurutani, B. T., Park, S. A., Falkowski, B. J., Bortnik, J., Lakhina, G. S., Sen, A., et al. (2019). Low frequency (f < 200 Hz) polar plasmaspheric hiss: coherent and intense. *Journal of Geophysical Research: Space Physics*, *124*. https://doi.org/10.1029/2019JA027102

Received 29 JUN 2019
Accepted 10 OCT 2019
Accepted article online 11/23/19



**Abstract** Low frequency (LF) ~22 Hz to 200 Hz plasmaspheric hiss was studied using a year of Polar plasma wave data occurring during solar cycle minimum. The waves are found to be most intense in the noon and early dusk sectors. When only the most intense LF (ILF) hiss was examined, they are found to be substorm dependent and most prominent in the noon sector. The noon sector ILF waves were also determined to be independent of solar wind ram pressure. The ILF hiss intensity is independent of magnetic latitude. ILF hiss is found to be highly coherent in nature. ILF hiss propagates at all angles relative to the ambient magnetic field. Circular, elliptical, and linear/highly elliptically polarized hiss have been detected, with elliptical polarization the dominant characteristic. A case of linear polarized ILF hiss that occurred deep in the plasmasphere during geomagnetic quiet was noted. The waveforms and polarizations of ILF hiss are similar to those of intense high frequency hiss. We propose the hypothesis that ~10–100 keV substorm injected electrons gradient drift to dayside minimum B pockets close to the magnetopause to generate LF chorus. The closeness of this chorus to low altitude entry points into the plasmasphere will minimize wave damping and allow intense noon-sector ILF hiss. The coherency of ILF hiss leads the authors to predict energetic electron precipitation into the mid latitude ionosphere and the electron slot formation during substorms. Several means of testing the above hypotheses are discussed.

## 1. Introduction

Plasmaspheric hiss is an electromagnetic whistler mode wave with a frequency range between ~20 Hz and ~2.0 kHz, observed by satellites inside the plasmasphere and inside plasma plumes (Russell et al., 1969; Thorne et al., 1973). Thorne et al. (1973) named the waves "hiss" for the sound it made when played through a loudspeaker. Since the original first observations of these plasma waves, there have been a plethora of publications on this wave mode, particularly more recently related to the data taken from the THEMIS and Van Allen Probes missions (Thorne et al., 1973, 1977, 1979, Thorne, 2010; Smith et al., 1974; Tsurutani et al., 1975, 2012, 2015, 2018; Carpenter, 1978; Cornilleau-Wehrlin et al., 1978, 1993; Kokubun, 1983; Solomon et al., 1988; Gail & Inan, 1990; Storey et al., 1991; Dragonov et al., 1992; Santolik et al., 2001, 2002, 2006, Santolik, 2008; Shinbori et al., 2003; Parrot et al., 2004; Meredith et al., 2004, 2006, 2007, 2018; Green et al., 2005; Summers et al., 2008, 2014; Bortnik et al., 2008, Bortnik, Li, et al., 2009, Bortnik, Thorne, & Meredith, 2009, Bortnik et al., 2011; Santolik & Chum, 2009; Breneman et al., 2009; Chen et al., 2009, 2012, 2014; Wang et al., 2011; Delport et al., 2012; Agapitov et al., 2013, 2014, 2018; Li et al., 2013, Li, Chen, et al., 2015, Li, Ma, et al., 2015, Li et al., 2017, 2019; Glauert et al., 2014; Kim et al., 2015, Kim & Shprits, 2019; Spasojevic et al., 2015; Gao et al., 2015, 2018; Malaspina et al., 2016, 2017, 2018; Falkowski et al., 2017; Yu et al., 2017; Shi et al., 2017, 2018, 2019; Kavanagh et al., 2018; Su et al., 2018; Zhang et al., 2018; Zahlava et al., 2018; Nakamura et al., 2018; Hartley et al., 2018, 2019; Ni et al., 2017, 2019; Zhao et al., 2019; Hua et al., 2019; He et al., 2019; Teng et al., 2019). The continued strong interest in plasmaspheric hiss and plasma plume (Chen & Grebowsky, 1974) hiss has partly been due to the complexity of the sources of the emissions and partly due to findings of new features. In the above references, hiss in the plasmasphere has been detected during geomagnetic quiet, during substorms and storms and during solar wind pressure pulses. All those dependences implying several different generation mechanisms are contributing to hiss-like waves inside the plasmasphere. Some of plasmaspheric hiss may come from outer

zone chorus propagating into the plasmasphere (there are also arguments for why this does not occur), wave circulation and amplification within the plasmasphere (Thorne et al., 1979), and direct generation through energetic particle injection into the plasmasphere with local plasma instability (Cattell et al., 2015; Kennel & Petschek, 1966; Lakhina et al., 2010; Li et al., 2013) generating the waves. Dispersion and decay of lightning generated sferics (Dragonov et al., 1992; Ni et al., 2017) and magnetosonic waves have also been mentioned as possible sources of hiss (Meredith et al., 2006; Sonwalkar & Inan, 1989).

Recently, Li et al. (2013) discovered a low frequency component of plasmaspheric hiss during a substorm that occurred on 30 September 2012. They argued that hiss frequencies down to ~20 Hz were unlikely to be caused by the inward propagation of chorus and argued that this event must be due to energetic ~100 keV electrons injected into the high plasma density plasmasphere with local generation occurring within that body. Chen et al. (2014) added to this scenario and mentioned that the gain from cyclical raypaths could account for the measured wave intensities. Li, Ma, et al. (2015) indicated that the low frequency hiss can increase ~100 keV electron pitch angle scattering rates substantially, and this emission should be added to future models of radiation belt electron dynamics. A new twist has been added by Shi et al. (2018). They show a strong low frequency plasmaspheric hiss correlation with Ultra Low Frequency (ULF) wave oscillations. Those authors suggested that the ULF waves are modulating energetic electron distribution functions, which in turn through instability, are generating the hiss. This is similar to the suggestions of Tsurutani et al. (2015, 2018) and Falkowski et al. (2017) who detected intense and coherent hiss inside plasma plumes and suggested that higher wave growth rates were necessary to explain the presence of hiss in these regions. Circulation models cannot be applied for such small regions of space. Recent works on hiss within plumes (Hartley et al., 2019; Li et al., 2019; Nakamura et al., 2018; Shi et al., 2019; Teng et al., 2019; Zhang et al., 2018), although not the main focus of this paper, will be commented on in sections 4 and 5 of this paper in this light.

There have been two new surveys that have studied low frequency plasmaspheric hiss from a statistical point of view, giving the readership the general properties of these waves. Malaspina et al. (2017) have used ~2 ½ years of Van Allen Probes search coil data to study hiss with frequencies between ~40 and 150 Hz. They compare these results to higher frequency hiss, defined as hiss waves in the frequency range from ~150 Hz to 2.0 kHz. They show clear examples of two separate bands of hiss existing at the same time. The two bands increase and decrease in power together and have approximately the same amplitude. However one main difference is that the low frequency hiss has peak amplitudes at ~15 MLT, while the high frequency hiss peaks near 12 MLT. This latter observation gives hints on the generation mechanism of both frequency types of hiss.

Meredith et al. (2018) also performed a statistical study of both high frequency and low frequency plasmaspheric hiss using data from eight satellites. They found that hiss is, in general, most intense on the dayside and increases with geomagnetic activity from midnight to dawn through noon to dusk. Hiss was most intense in the 200–500 Hz range at high AE (in agreement with statistical results of Tsurutani et al., 2015). This could be due to chorus origin. However low frequency hiss (defined as ~50 to 200 Hz) peaks prenoon at the equator and decreases with increasing magnetic latitude (MLAT) for low L values. They argue that this is inconsistent with chorus origin and more consistent with substorm injected energetic electron local generation. Meredith et al. (2018) also mention that in the premidnight sector for all hiss (~50 Hz to 1.0 kHz), their intensities decrease with increasing AE. They argue that chorus at large L in the postnoon sector enters into the plasmaspheric bulge region and then propagates eastward inside the plasmasphere.

The purpose of the present study will be focused on low frequency (LF) plasmaspheric hiss and LF plume hiss (defined as ~22 to 200 Hz) using ~1 year of Polar plasma wave data during solar minimum (where there was a general lack of magnetic storms). This study will be complementary to the recent Tsurutani et al. (2018) study that focused only on high frequency (HF) (defined as ~300 Hz to 1.0 kHz) plasmaspheric hiss. The present study will make comparisons between the present results and those previously of HF hiss in Tsurutani et al. (2018) and those of the recent Malaspina et al. (2017) and Meredith et al. (2018) surveys. This new study will also have unique aspects not covered by Malaspina et al. (2017) and Meredith et al. (2018). If the LF hiss source is different than the HF hiss source, are the waveforms unique in any aspect? Second, our survey will focus on different hiss features, particularly the coherency and detailed properties of the waves.

Following the Tsurutani et al. (2018) work, we will focus on the ten most intense LF plasmaspheric hiss wave events, separately in each of four magnetic local time (MLT) sectors: midnight (21 < MLT < 03), dawn (03 < MLT < 09), noon (09 < MLT < 15), and dusk 15 < MLT < 21). For brevity, we will call the intense LF (ILF) hiss. From these 40 events, we will identify hiss spatial locations, hiss coherency, and directions of propagation from five-wave cycle and from single wave cycle events. Substorm dependence of these intense hiss events (AE* and SYM-H* dependences, where the "*" designates incorporation of gradient drift time delays of ~25 keV electrons) will also be studied. The ILF plasmaspheric hiss dependence on the solar wind ram pressure will be determined using upstream solar wind data. The wave polarization (circular, elliptical, and linear/highly elliptical) as a function of spatial location will be studied to obtain further information on the wave sources.

## 2. Method of Data Analyses

In this study, we consider LF plasmaspheric hiss in the frequency range from ~22 Hz to ~200 kHz using ~1 year of Polar satellite data (April 1996 to April 1997). For certain of the wave properties,, we will compare them to HF plasmaspheric hiss (~300 Hz to 1.0 kHz) results which were previously published in Tsurutani et al. (2018). The waves between 200 Hz and 300 Hz were omitted from this present study to avoid possible HF hiss contamination of the present LF hiss study. The purpose of the comparison will be to identify different features which may give clues to the source of origin of LF plasmaspheric hiss. The LF hiss data can be obtained at NASA's CDAWeb (http://cdaweb.gsfc.nasa.gov).

The Polar plasma wave instrument (PPWI) and data are described in Gurnett et al. (1995). The average wave log intensities are used for the statistical part of the study. Magnetosonic waves and chorus were removed from the data set as described in Tsurutani et al. (2014).

The high frequency waveform receiver (HFWR) 2 kHz bandwidth data were used for the statistical studies. These data cover the frequency range from ~22 Hz to ~2 kHz. The ~2 min intervals were used for our statistical studies and will be called "intervals" in the text. A "wave event" occurs if LF plasmaspheric hiss is detected during an interval. Bin sizes of 1 L by 1-hr MLT resolution are used in this study. The average LF plasmaspheric hiss crossing event was ~98 min. The minimum time was ~60 min, and the maximum time was ~173 min. These crossing time values are due to a combination of the Polar trajectory through the wave region and the actual hiss duration.

The data set under study is the same as that used by Tsurutani et al. (2018) to study ~300 Hz to 1.0 kHz HF and intense HF (IHF) plasmaspheric hiss. Approximately 800 passes occurred when the ~2 kHz satellite wave data were available. There are many ~2 min "intervals" and thus many potential LF hiss events. These data are the bases for the statistical portion of our analyses.

The ten most ILF hiss ~2 min wave events in each of four local time sectors (midnight 21 to 3 MLT, dawn 3 to 9 MLT, noon 9 to 15 MLT, and dusk 15 to 21 MLT) will be identified. The purpose will be to study not only the specific ~2 min interval intense wave event but also the ILF plasmaspheric hiss throughout the satellite pass for that event. This satellite pass data will be called "an ILF plasmaspheric hiss interval". From this database, the LF hiss at different MLTs and MLATs will be compared. These data will be used to also identify substorm and solar wind pressure dependences of these particularly ILF hiss events.

A ~0.4 s snapshot which contains high time resolution three-axis magnetic wave components is obtained for every ~2 min interval (Santolik et al., 2001). We will use the high time resolution ~0.4 s LF plasma wave data for our case studies. To determine the LF wave **k** (the direction of wave propagation), the minimum variance method (Smith & Tsurutani, 1976) is used. A cross-correlation analysis between the B2 (intermediate variance) and B1 (maximum variance) is used to determine wave coherence for the above 40 ILF hiss cases of 10 maximum wave intensities (in the 4 MLT sectors). The analyses were performed first on the entire ~0.4 s interval, second on a selected five-wave cycle sample within each event, and third on each individual cycle of the five-wave cycle interval. This was done for all 40 ILF plasmaspheric hiss intervals. Thus we have examined 200 individual wave cycle events as described above. We determine the wave ellipticity and also the wave direction of propagation relative to the ambient magnetic field. This last parameter is called $\theta_{kB}$ in the paper.

The ILF hiss wave ellipticity is determined by the hodograms of the wave minimum variance B1 and B2 components. The wave handedness is obtained from the wave **k** direction, the ambient magnetic field direction, Bo (determined from the d.c. magnetometer data), and the B1 versus B2 hodogram. The wave **k** direction is taken as the minimum variance direction, B3 (Verkhoglyadova et al., 2010). The ambient magnetic field Bo is used to determine $\theta_{kB}$, but is not explicitly shown in the paper.

The wave coherency is determined by cross correlating the B1 and B2 components. This technique was developed in Tsurutani et al. (2009 & 2011). It has been demonstrated that wave-particle cyclotron resonant interactions involving coherent waves will have ~$10^3$ greater pitch angle diffusion rates than that with incoherent waves (Bellan, 2013; Lakhina et al., 2010; Tsurutani et al., 2009, 2011).

It should be noted that the wave **k** is well determined to be in the direction of minimum variance B3 for circularly polarized and elliptically polarized waves (Verkhoglyadova et al., 2010). Elliptical polarizations will be shown to be the most common type of LF hiss waves. The minimum variance technique and wave **k** determination is not accurate for linearly polarized and highly elliptically polarized waves. However the results of applying this technique for such waves will be shown for completeness. There is no known technique for identifying **k** for linearly polarized/highly elliptically polarized waves using analyses of wave magnetic data alone at this time.

The data for this study were obtained during solar minimum. During this phase of the solar cycle, there is typically a minimum number of intense Interplanetary CME (ICME)-generated or sheath-generated magnetic storms (Echer et al., 2008; Gonzalez et al., 1994; Tsurutani et al., 1988). The high-speed stream-slow-speed stream interactions form corotating interaction regions (CIRs: Smith & Wolfe, 1976) at their interfaces. CIRs can possibly cause weak magnetic storms (Echer et al., 2008; Tsurutani et al., 1995). The high-speed streams sunward of the CIRs are the dominant interplanetary feature resulting in geomagnetic activity during this part of the solar cycle. The southward IMF components of embedded Alfvén waves within these solar wind phenomena are responsible for high-intensity long-duration continuous AE activity (HILDCAA) events (Hajra et al., 2013, 2014; Tsurutani et al., 1995, 2004, 2006; Tsurutani & Gonzalez, 1987), a series of intense substorms/small injection events. These substorms/small injection events lead to midnight sector plasma sheet injections of ~10 to 100 keV anisotropic electrons into the magnetosphere and the generation of chorus waves (Tsurutani et al., 1979; Tsurutani & Smith, 1974).

A study the 40 intense LF plasmaspheric hiss events was performed using the solar wind ram pressure calculated from solar wind velocity and density measurements. The latter are taken from the OMNI website. Since solar wind pressure has an immediate effect on the betatron acceleration of the energetic ~10–100 keV electrons in the dayside outer magnetosphere, no further time delays were used. When we consider ILF plasmaspheric hiss associated with substorms and energetic electron injection events, the AE and SYM-H values are used assuming midnight injection with further gradient drift of the energetic electrons to the local time of detection. A model of gradient drift of ~25 keV electrons is used for determining the time delays. This model was found to be a good measure of chorus delay times by Tsurutani and Smith (1977) and more recently by Falkowski et al. (2017) and Tsurutani et al. (2018). We will refer to the precursor AE and SYM-H values in this paper as AE* and SYM-H*. The AE and SYM-H data were obtained from the WDC at Kyoto University (http://wdc.kugi.kyoto-u.ac.jp/wdc/Sec3.html).

A recap of terminology used in this paper may be useful to the reader. ~2 min 2 kHz bandwidth data are called “intervals”. If LF plasmaspheric hiss is detected within the interval, it is called a “hiss event.” These 2 min intervals/events are used for the statistical studies in this paper. The top ten most intense LF 2 min hiss events were then selected for each of four MLT sectors. These intense LF hiss events are called ILF hiss. These wave events were selected so all occurred during different satellite passes. For these events, the adjacent 2 min events were identified, etc., so that the data for the particular satellite pass were identified. This is called an event interval, and additional statistics is performed on these data. Associated with each 2 min wave event are ~0.4 s waveform data. These data are used for the detailed studies of the ILF hiss waves. We will analyze the 0.4 s data, 5 selected consecutive wave cycles within the 0.4 s data, and individual wave cycles of the five-wave cycle intervals.

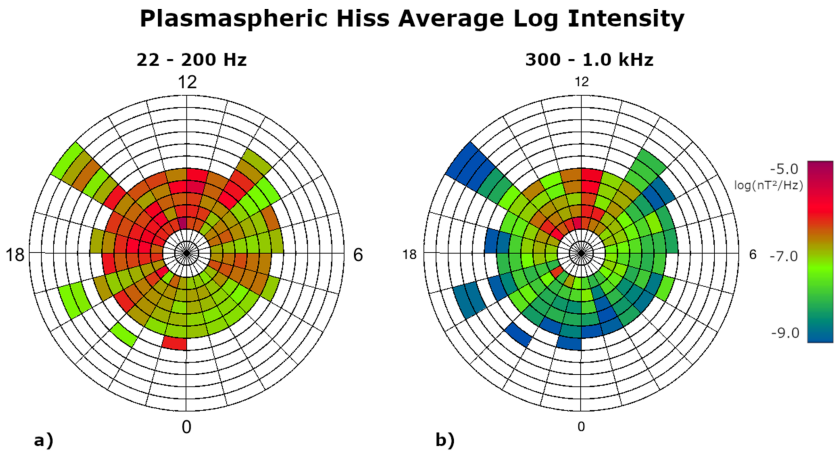


**Figure 1.** A comparison of the intensity and location of LF plasmaspheric hiss (~22 to 200 Hz), panel a), to HF plasmaspheric hiss (~300 Hz to 1.0 kHz), panel b) for the 1-year Polar study. For both panels, noon is on the top, and dusk is on the left. The coverage extends from L = 2 to L = 13. The legend on the right gives the average of the log intensities of 2 min intervals for each ΔL-ΔMLT bin. The bin size is 1 hr MLT and 1 L shell. Panel (b) was taken from Tsurutani et al. (2018).

The solar wind data was obtained from the OMNI website (http://omniweb.gsfc.nasa.gov/). This data was time-adjusted to take into account the solar wind propagation time from the spacecraft to the magnetosphere, so no further adjustments were made to the data.

## 3. Results

### 3.1. LF Plasmaspheric Hiss L and MLT Distribution

Figure 1 shows a comparison of the survey of LF plasmaspheric hiss (left panel) to HF plasmaspheric hiss (right panel) for the two 1-year studies. The LF hiss distribution is from this study, and the HF plasmaspheric hiss distribution is taken from Tsurutani et al. (2018). The log intensity scale is given on the right and is the same for both panels. The main features are that both LF and HF hiss are most intense in the dayside sector. The LF hiss is more intense by an order of magnitude than the HF hiss. The dayside peak intensity locations of both the LF and HF hiss are in agreement with the Meredith et al. (2018) results. Meredith et al. (2018) who used average intensities for all hiss in their study determined that LF and HF hiss had approximately the same intensities.

The LF hiss intensity maximum extends more toward dusk, shifting the center of the peak closer to postnoon. This latter feature is in agreement with the Malaspina et al. (2017) results.

It should be noted that the hiss for L > 7 at all MLT are detected (but with different intensities) in both the LF and HF hiss surveys. We presume these to be hiss in plasma plumes. It is found that when hiss is detected in plumes, it is detected as a broad frequency band emission covering both the LF and HF ranges. However it should be noted by the reader that chorus in plumes may have been eliminated from the data set by the data set "cleaning" process mentioned in section 2. More will be stated about this later.

The ten most intense ~2 min average hiss intervals for each of the four MLT sectors were identified as described in section 2. Figure 2a shows the 40 most intense ~2 min LF plasmaspheric hiss average log intensity interval locations in L and |MLAT|. As mentioned previously, the 40 events are composed of the top 10 most intense events for each of 4 local time sectors: noon, dusk, midnight, and dawn. What is interesting in this panel is that the highest intensity intervals (red and orange) are distributed relatively evenly over all |MLAT| values from 0° to 40°. The most striking feature of this distribution is that the ILF hiss is quite predominant at large L ($5 \leq L \leq 7$) at relatively high |MLAT| ($25° \leq |MLAT| \leq 40°$). This latitude distribution is somewhat in contrast to those of Meredith et al. (2018), but it should be remembered that this is for only

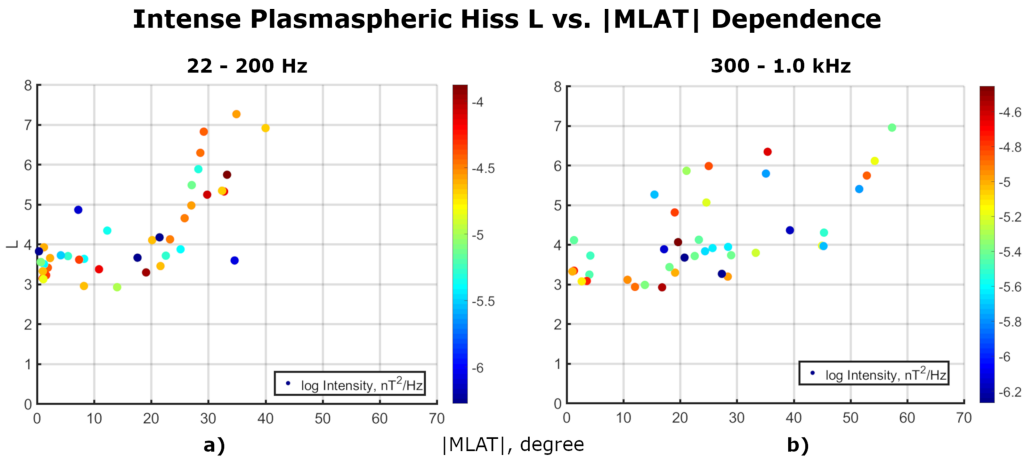


**Figure 2.** A comparison of the |MLAT| location of the 40 most intense ~2 min intervals of LF plasmaspheric hiss versus L (panel a) to the 40 most intense ~2 min intervals of HF plasmaspheric hiss (panel b). The color scales for the log intensities are on the right of each panel. It should be noted that the two scales are slightly different in this figure. Panel (b) is taken from Tsurutani et al. (2018).

high-intensity LF plasmaspheric hiss and not for all events. Also the Meredith et al. results were limited to very low L values.

Figure 2b shows the 40 most IHF plasmaspheric hiss L and |MLAT| distribution for comparison. It is in general similar to the ILF hiss in that the red orange events are spread over all values of |MLAT| from 0° to 60°. Note that these IHF events extend to higher |MLAT| values than do the ILF hiss.

The Polar spacecraft L-|MLAT| coverage was shown in Figure 3b of Tsurutani et al. (2018) and will not be repeated here. However it should be stated that Polar covers the magnetic equator well between L = ~2.4 and ~4.3, but not for higher L. At L = 6 to 7 (the nominal plasmapause location), Polar covers the MLAT range of ~20° to ~40° well. However at lower and higher MLATs outside this range, the coverage is poor to nonexistent.

### 3.2. The Detailed Properties of the 10 Most Intense LF Plasmaspheric Hiss ~2 min Intervals in the Four MLT Sectors

The ten most intense ~2 min average LF plasmaspheric hiss intervals for each of the four MLT sectors were identified and their L, |MLAT|, and log intensity values were previously shown in Figure 2a. These 40 intervals were examined in greater detail using the high time resolution waveform data. Each interval was found to be composed of many small intervals (approximately five wave cycles) of coherent waves. Totally incoherent waves were not detected within the 40 ~2 min intervals studied. Although not examined, lower intensity plasmaspheric hiss may also be coherent in nature. This effort is beyond the scope of the present study.

All of the clearly identifiable waves were determined to be right-hand polarized. All types of polarizations were detected: circular, elliptical, and linear/highly elliptical. No apparent local time dependences for these three general polarizations were found. Examples of each of these three types of right-hand wave polarizations are shown below.

### 3.3. Polarizations of Whistler Mode Plasmaspheric Hiss

Figure 3 is an example of a mixture of polarizations of ILF plasmaspheric hiss occurring within a 0.4 s interval. The ILF hiss occurred at L = .6.9, a MLT of ~7.8 (local dawn sector), and a MLAT of ~40.0°. The event started on 27 July 1996 at ~0758:03.545 UT. The wave interval occurred during moderate geomagnetic activity with AE* = 326 nT and SYM-H* = 16 nT. From top to bottom are the wave magnetic field B1 (maximum variance) component, the B2 (intermediate variance) component, the B3 (minimum variance) component, and B magnitude. The bottom left box displays the B1-B2 hodogram and the bottom right box the B1-B3 hodogram.

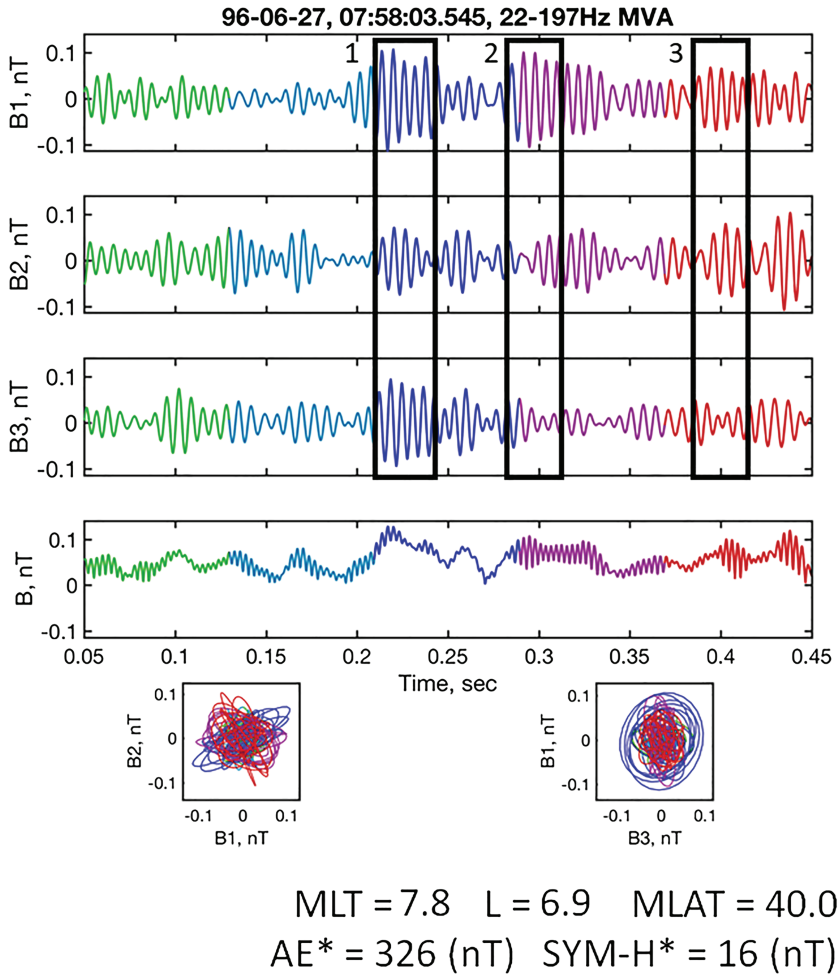


**Figure 3.** A ~0.4 s interval with a variety of wave polarizations. Five different colorizations with equal time intervals have been used to allow the reader to follow the evolution of the waves. The top four plots are the magnetic field components in minimum variance coordinates and the wave magnetic field magnitude variations. The bottom two plots are the B1-B2 and B3-B1 hodograms. The event occurred on June 27, 1996.

Three separate cases of five-wave cycle intervals are indicated by rectangles and labeling 1, 2, and 3. In case 1, there are strong wave amplitudes for all three (B1 through B3) magnetic field components indicating that the minimum variance direction for this wave packet is different than for the whole interval. This will be discussed further later. In case 2, the wave packet starts with B1 amplitudes clearly the largest, ~ ±0.1 nT, and B2 and B3 with much smaller amplitudes. The first two wave cycles are thus linearly polarized. From cycles 3 to 5, B1 decreases to ~ ±0.07 nT and B2 increases to ~ ± 0.04 nT, indicating elliptical polarization. In case 3, the B1 and B2 wave amplitudes are essentially equal at ~ ±0.05 nT and the B3 variation negligible. This indicates wave circular-to-elliptical polarization.

The left-hand hodogram, plotting B1 versus B2, shows several planes of ellipticity. This is consistent with a variety of orientation of the waves. One possible interpretation is that the wave packets are coming from substantially different directions (we will show that with even more detailed analysis, this is the case). The results of this analysis also indicate that one should take care in determining wave polarizations. If one simply uses long time scale averages such as the whole ~0.4 s interval in Figure 3, the results will give only the average properties and miss the details of the waves. We will argue that much shorter time scales are needed. Single-wave cycle analyses will be shown to be best.

The five-wave cycle interval of case 1 (Figure 3) is displayed in Figure 4 in minimum variance coordinates calculated for only this interval. The start of the interval is at 07:58:03.7 UT. The left-hand panels

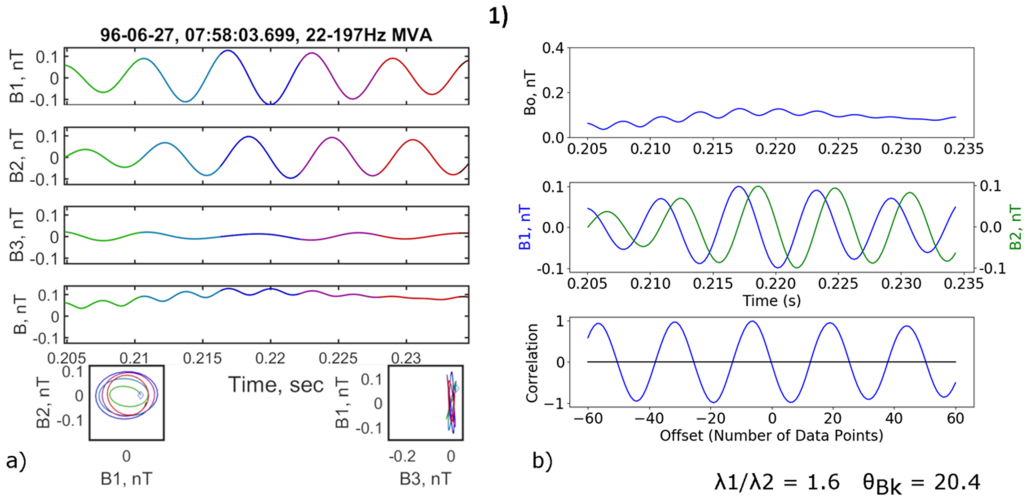


**Figure 4.** Panel (a) five cycles of ILF plasmaspheric hiss. Figure 3 format is used. This is case 1 in Figure 3. Discrete coloration has been used to identify different portions of the wave interval. At the bottom of panel (a) are two hodograms indicating the wave polarization (left side) and wave planarity (right side). In Panel (b), the top panel gives the wave field magnitude variations. The second panel gives the B1 (blue) and B2 (green) components. The bottom panel shows the cross correlation of B1 and B2 results.

(Figure 4a) are given in the same format as in Figure 3. The B1 amplitude is ~ ±0.12 nT, the B2 amplitude ~ ± 0.11 nT, and the B3 amplitude ~ ±0.01 nT, indicating almost circular polarization. There is a wave phase shift between B1 and B2 of ~90°. The B1-B2 hodogram at the bottom left confirms that the wave polarizations are slightly elliptical. The eigenvalue ratio $\lambda1/\lambda2 = 1.6$. The B1-B3 hodogram indicates that these are planar waves. The waves are propagating at an angle of ~21° relative to the ambient magnetic field direction.

Figure 4b from top to bottom gives the wave magnetic field magnitude variations, B1 (blue) and B2 (green) components (plotted superposed in the same panel), and the cross correlation between B1 and B2. The bottom graph clearly shows that the waves are coherent with a ~0.9 cross-correlation coefficient.

Figure 5 is an examination of the five wave cycles of case 2 in Figure 3, starting at 07:58:03.8 UT. Even though the minimum variance calculation was done for only this interval, one can tell from panel (a) that the wave direction of propagation was changing even during this five-wave cycle packet. There is a change from a reasonably large oscillation in B3 for the first two cycles and then in B2 for the last three cycles. This means that one really needs to examine each individual wave cycle. By analyzing five cycles at the same time, this is providing results which are based on the average properties. Analysis of individual cycles will provide different results. One can note from the B1-B2 hodogram that the beginning interval (green and blue) is originally highly elliptically polarized and the last three cycles (red) are less elliptical. The value $\lambda1/\lambda2$ was 4.3. The average angle of propagation of the waves relative to the ambient magnetic field was 59.5°. Notice that the previous wave packet direction was 20.5° degrees relative to the ambient magnetic field, so the supposition of a superposition of waves coming from different directions is verified.

The cross-correlation results in Figure 5b show that the waves are quasi-coherent. It should be noted that this technique of correlating B1 and B2 to study wave coherency will not work for linearly polarized waves.

Figure 6 gives an example of ~0.4 s of linearly polarized waves occurring at a MLT of 7.1 (near dawn), at a L of 3.4 with a MLT of ~2.0°. The AE* value was 101 nT and SYM-H* −5 nT, indicating almost geomagnetic quiet. Panel (a) shows several wave packets with peak amplitudes of ~±0.2 nT in the B1 component. There is little or no variation in B2 and B3. The B1-B2 hodogram shows that the waves are linearly polarized. There are many "wave packets" throughout the entire ~ 0.4 s interval. They are all linearly polarized.

What is interesting is this is a substantial event spanning from ~80 Hz to ~300 Hz covering both LF and HF hiss ranges (not shown). The intensities of both LF and HF hiss are close to $10^{-4}$ $nT^2/Hz$. By measuring the five wave cycles in the box of B1 in panel (a), a rough frequency of ~100 Hz is determined. This is almost in

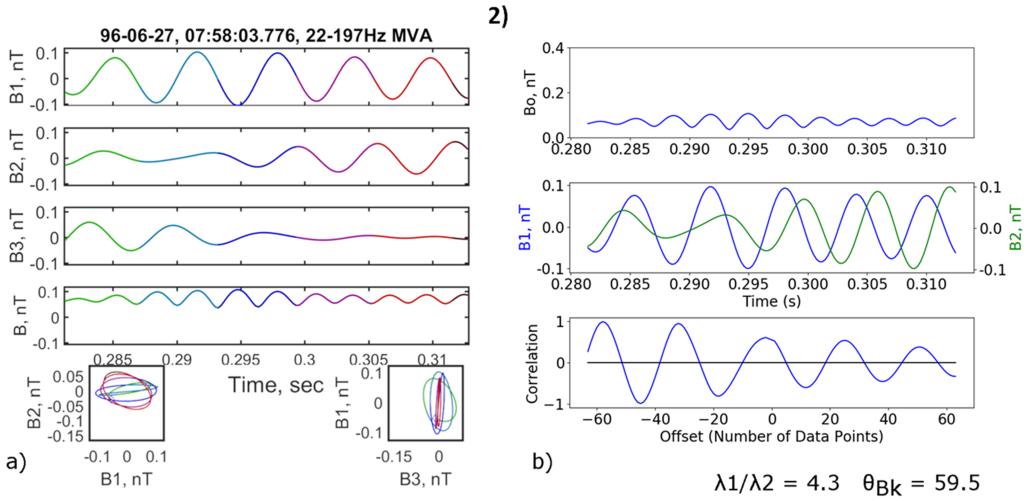


**Figure 5.** A 5 wave cycle interval of ILF hiss that contains elliptically/linearly polarized waves. The format is the same as in Figure 4. This is case 2 in Figure 3.

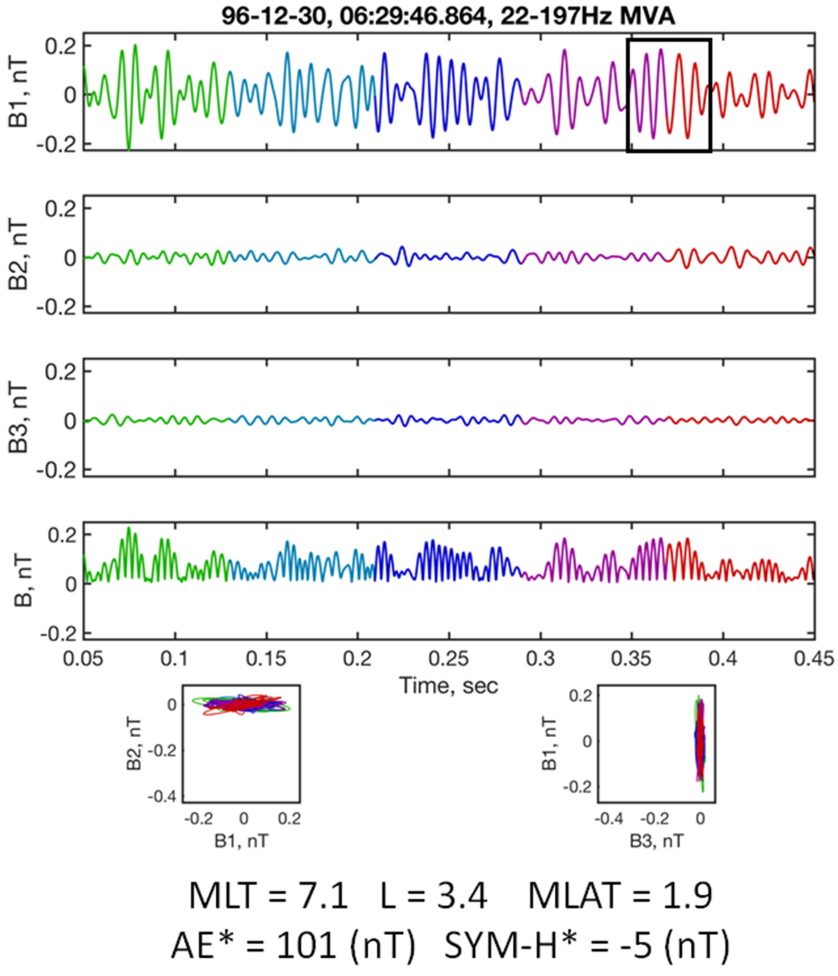


**Figure 6.** Same format as in Figure 3 for an ILF wave interval that occurred on 30 December 1996. An example of a ~0.4 s interval with several packets of linearly polarized low frequency waves.

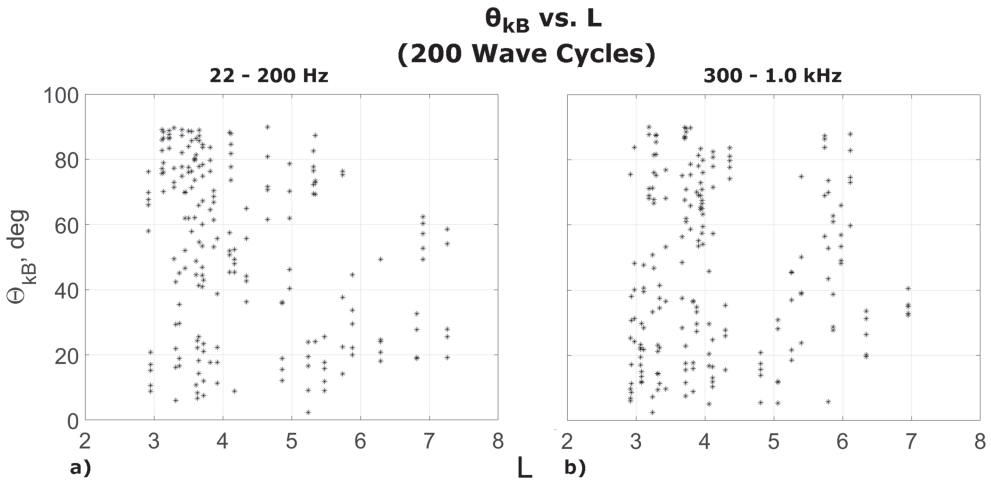


**Figure 7.** The wave normal direction (k) relative to the ambient magnetic field versus L for ILF hiss (panel a) and for IHF hiss (panel b). Panel (b) is reproduced from Tsurutani et al. (2018).

the midrange of the intense, long-duration ~30 min event. The properties of the waves (linearly polarized), and occurring at the magnetic equator, make this event appear to be quite similar to magnetosonic waves (see Tsurutani et al., 2014). However, it is noted that this event occurred deep in the plasmasphere (L = 3.4) during geomagnetic quiet (AE* = 101 nT). This event was identified because it was one of the ten most intense events detected in the dawn MLT range. Clearly similar LF wave events may be present in other statistical studies of LF plasmaspheric hiss.

All of the five wave cycles of the ten most Iintense LF events for each of the four MLT sectors were analyzed in detail. This is 200 cycles of ILF hiss. Figure 7a shows the ILF wave distribution of the angle of propagation $\theta_{kB}$ versus L. There are nearly parallel propagating waves ($\theta_{kB} < 20°$) for $3 < L < 7.5$. Waves with $80° < \theta_{kB} < 90°$ are detected primarily inside L = 5. However there are too few points to make a strong argument for these possible features being statistically significant. Our conclusion is that there appears to be no obvious pattern.

Figure 7b shows the IHF hiss for the same year of study. The $\theta_{kB}$ versus L distribution is similar in that there is no particularly clear pattern. The waves are detected at all $\theta_{kB}$ values for all L.

Although the ILF and IHF hiss databases extend from L = 2 to L = 13, it should be noted from Figure 7 that none of the most intense waves were found in the spatial regions $L < 3$ and $L > 7.5$. This means that although both LF and HF hiss were detected inside L = 3, the waves were not as intense as the highest intensities used

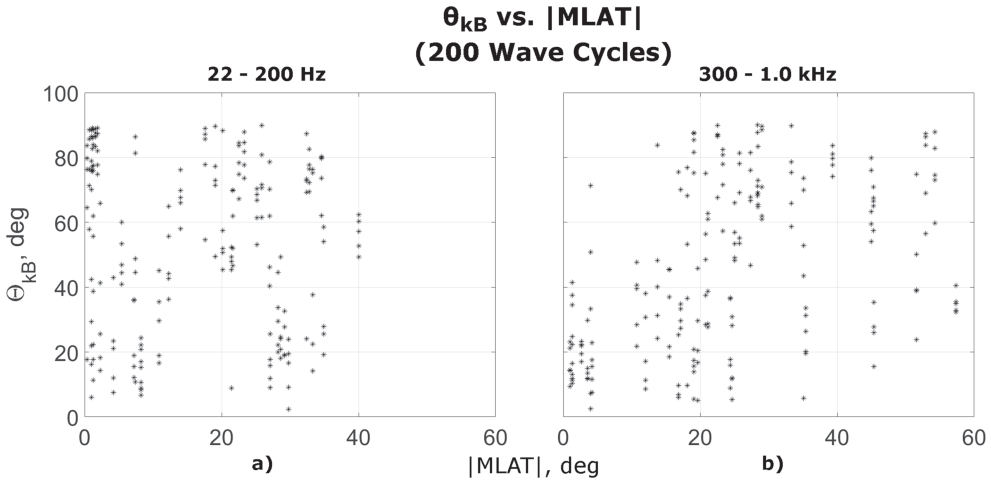


**Figure 8.** The wave angle of propagation $\theta_{kB}$ as a function of |MLAT|. Panel (a) gives the ILF hiss results, and panel (b) show the IHF results for comparison. Panel (b) was taken from Tsurutani et al. (2018).

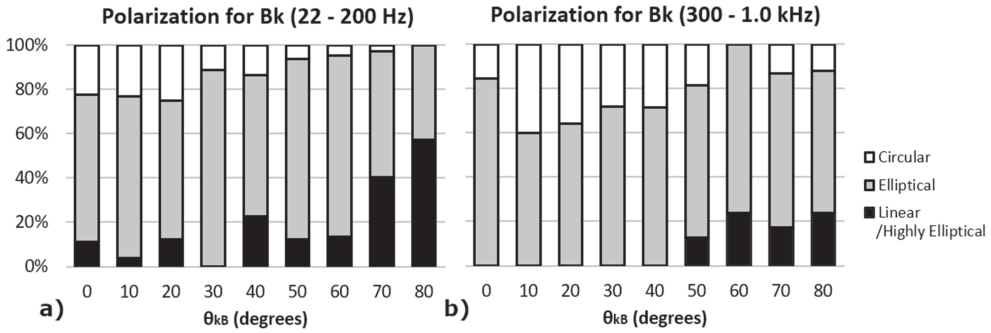


**Figure 9.** The percentage of circularly polarized, elliptically polarized, and linearly/highly elliptically polarized waves as a function of $\theta_{kB}$. Panel (a) gives the results for ILF plasmaspheric hiss. Panel (b) gives the results for IHF plasmaspheric hiss. The legend is on the right of panel (b). Panel (b) is taken from Tsurutani et al. (2018).

in this portion of the study. Waves inside plasma plumes (presumably for L > 7.5) were previously shown to be intense and coherent (Falkowski et al., 2017; Tsurutani et al., 2015, 2018), but clearly not as intense as the ILF events within the plasmasphere proper.

Figure 8a shows the 200 ILF hiss wave cycle angles of propagation $\theta_{kB}$ relative to the ambient magnetic field. These angles are plotted against the |MLAT| of the location of the spacecraft. The figure shows no obvious relationship between the two parameters. All values of $\theta_{kB}$ are detected at almost all |MLAT| values. Figure 8b shows the same for IHF plasmaspheric hiss. Again there appears to be no obvious dependences.

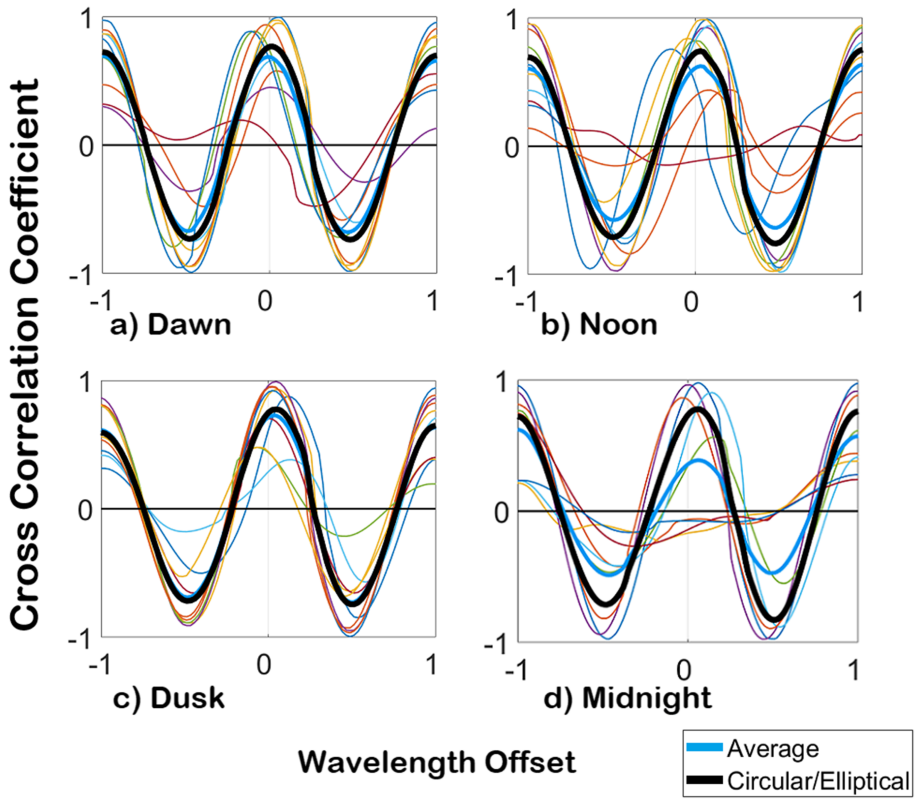


**Figure 10.** The coherency of ILF hiss waves in the four MLT sectors. In each of the four panels are plots of the cross correlations of the B1 and B2 minimum variance components of the 10–5 wave cycle intervals for two wavelength lags. Panels (a) through (d) are each of the ten most intense waves of each MLT sector: dawn, noon, dusk, and midnight. Individual events are displayed in color, and the average is indicated by the solid blue line. The average with linearly/highly elliptically polarized waves deleted is shown in the solid black line.

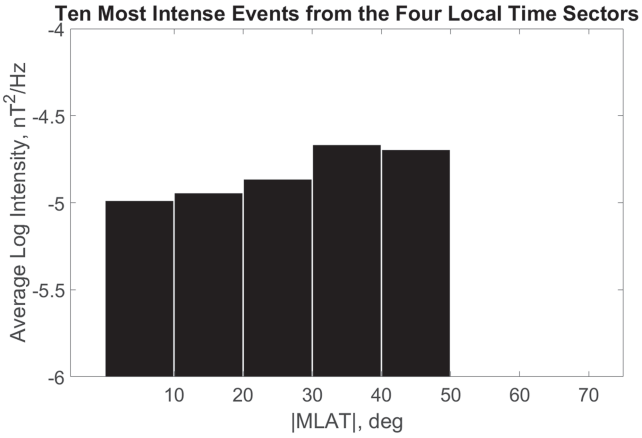


**Figure 11.** The average ILF hiss log intensities of all 40 ~2 min interval events averaged in 10° |MLAT| bins from 0° to 50°.

Figure 9a shows the percentage of circularly polarized (white), elliptically polarized (gray), and linearly/highly elliptically polarized (black) ILF hiss waves as a function of $\theta_{kB}$. What is readily apparent is that the majority of the single wave cycles are elliptically polarized in nature. There are circularly polarized waves which are detected at all $\theta_{kB}$ values but predominantly at small $\theta_{kB}$. There also linearly/highly elliptically polarized waves. They are present at all $\theta_{kB}$ values as well but predominately at large $\theta_{kB}$. The few events with apparent small $\theta_{kB}$ values were noted to be highly elliptical waves. The minimum variance technique does not work well for such wave polarizations, so the $\theta_{kB}$ values have large uncertainties. We left this data in the histogram for completeness.

Comparison of Figure 9a to 9b shows some minor differences of the ILF hiss from the IHF hiss. In Figure 9b, the waves are still primarily elliptically polarized. There were fewer circularly polarized ILF waves than for IHF waves. Conversely, there were more ILF linearly/highly elliptically polarized waves than IHF linearly/highly elliptically polarized waves.

Figure 10 shows two wavelength lags of cross correlations of the ten most ILF hiss and five-wave cycle intervals. The plot is the cross-correlation results from the wave B1 and B2 minimum variance components. The individual cycles in all four local time sectors show coherence to quasi-coherence. Typical cross-correlation values are ~0.8 to 1.0. There are some low correlation cases which can be noted in the dawn, noon, and midnight sectors. These are linearly/highly elliptically polarized wave events. The correlation results from those events are low as expected. This is especially true in the noon sector where there are three such events. These low correlation cases lower the average correlation results shown in the thick blue lines. The thick black lines are the averages without including the linearly/highly elliptically polarized events.

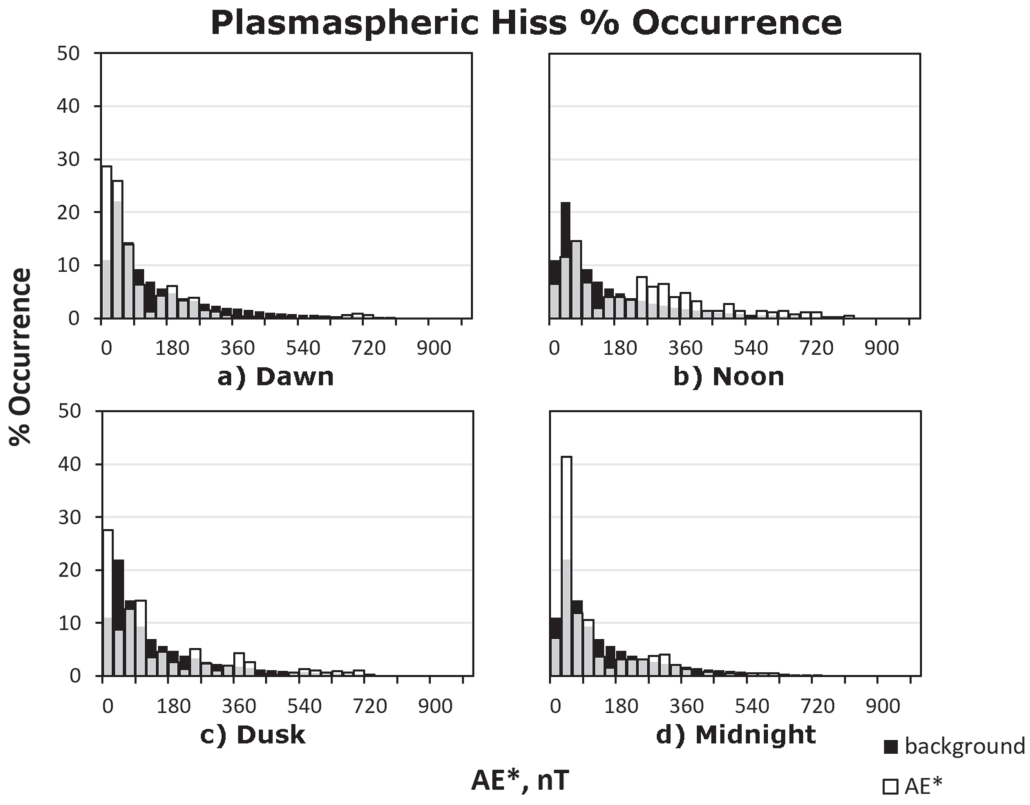


**Figure 12.** ILF high-intensity plasmaspheric hiss AE* distributions. From upper left clockwise are dawn, noon, midnight, and dusk sectors. The AE distribution for the year of study is shown in black, repeated in each panel.

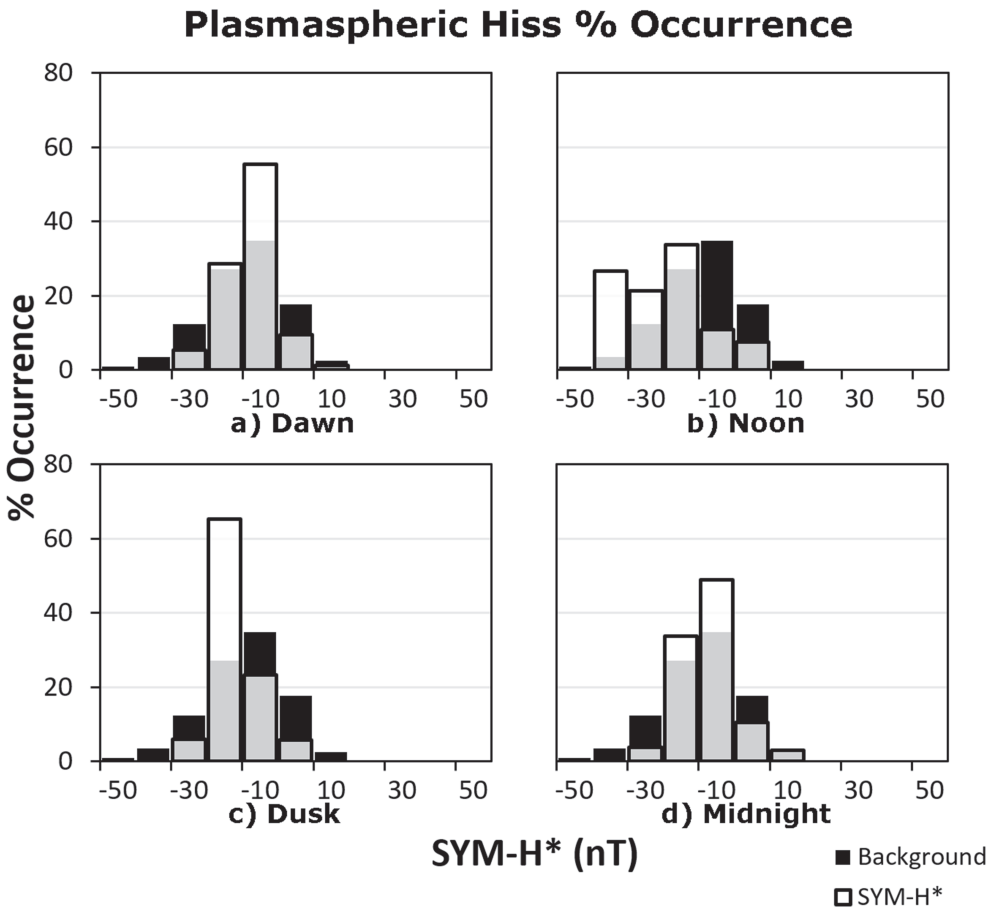


**Figure 13.** Same general format as in Figure 12 but for ILF plasmaspheric hiss event interval SYM-H* values. The four local time sectors are shown in the same sequence as in Figure 12. The SYM-H* ILF plasmaspheric hiss histograms are given in white/gray with the annual background SYM-H in black.

Each of the 40 ~2 min interval ILF hiss events was traced along the satellite orbit to identify the wave intensities for the entire satellite pass. This was described in section 2. Thus the database is considerably larger than 40 values. The ~2 min interval intensities were combined and subdivided into 10° |MLAT| bins. The average log intensity for each |MLAT| bin was calculated and is displayed in Figure 11. It is clear that the wave intensity is essentially the same, ~$10^{-5}$ $nT^2$/Hz from the magnetic equator to 50°.

It should be noted that the same result of a lack of a wave intensity versus |MLAT| dependence was found for IHF hiss in Tsurutani et al. (2018). The primary difference is that ILF hiss (above) has slightly higher intensities than the IHF hiss (~7 x $10^{-6}$ $nT^2$/Hz), consistent with other figures shown earlier in this paper.

### 3.4. Geomagnetic Activity and Solar Wind Ram Pressure Dependence of ILF Plasmaspheric Hiss

Figure 12 shows the ILF plasmaspheric hiss AE* distributions in four local time sectors. The panels are (a) the dawn sector, (b) the noon sector, (c) the dusk sector, and (d) the midnight sector. The ILF plasmaspheric hiss is given in percent occurrence in white, and the AE distribution percentage for the year is shown in black. When the ILF hiss percentage is higher than the yearly average percentage, the yearly average is indicated in gray. Similarly when the year AE average percentage is higher than the ILF hiss percentage, the latter is shown in gray.

We note that these results are suggestive (the best one can do) but are not definitive in a statistically significant way. Why do we say this? This is because one 2 min wave interval is not independent of adjacent 2 min

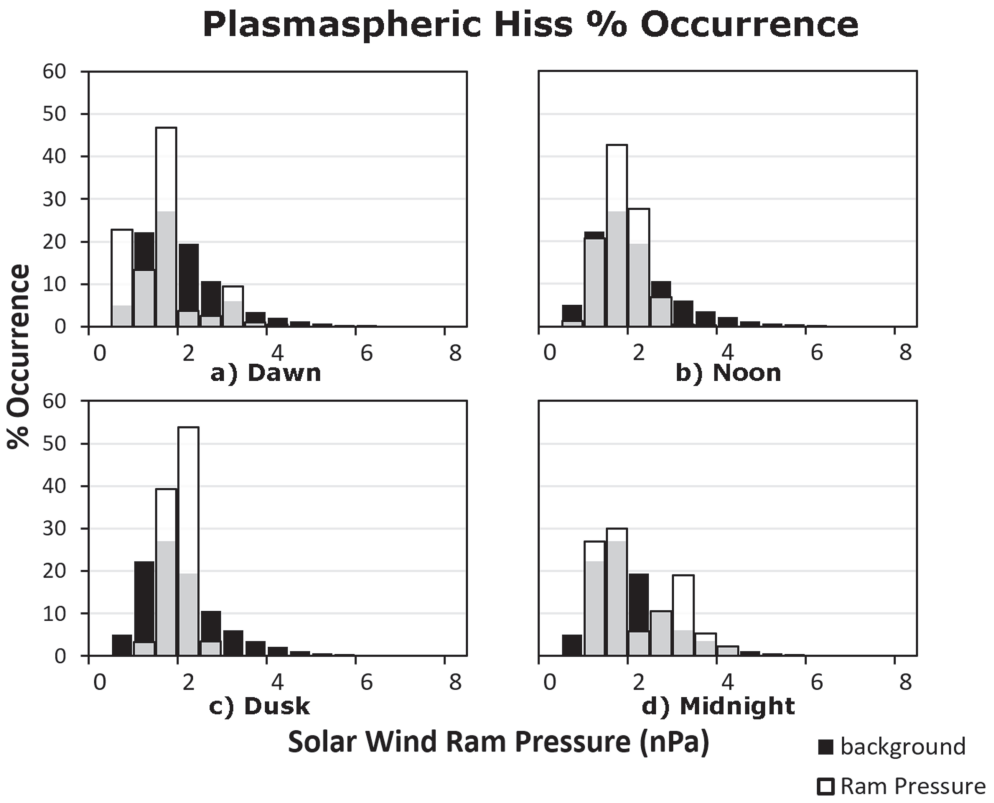


**Figure 14.** ILF plasmaspheric hiss solar wind ram pressure dependence. The format is the same as in Figure 13 but for ram pressure. The background solar wind ram pressure distribution is shown in each panel in black.

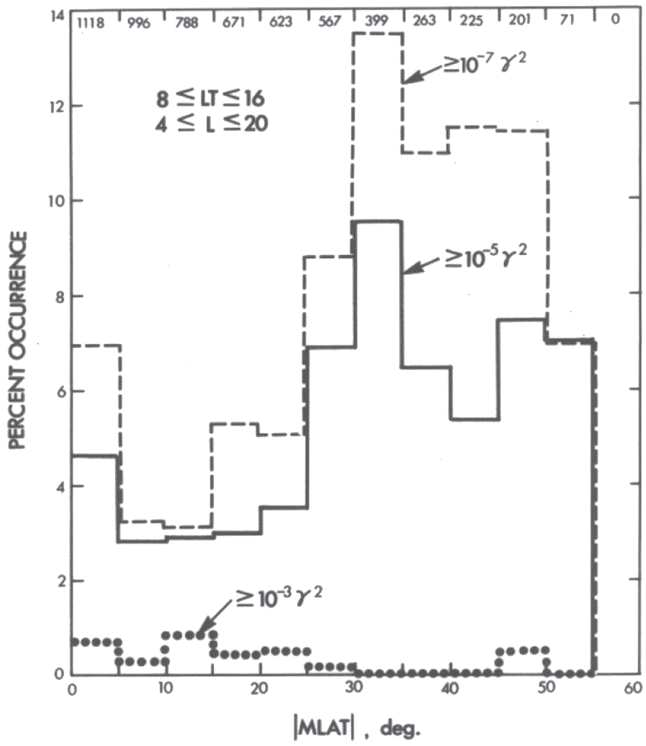


**Figure 15.** Outer zone chorus from a LT range of 08 to 16. Clearly intense chorus is present at high |MLAT| at values >30°. Taken from Tsurutani and Smith (1977).

intervals. The wave properties may "persist." In addition, the AE* values in adjacent 2 min intervals are also not independent from each other. This is a problem of all satellite plasma wave studies done in the past. None have been statistically significant. This comment also applies for Figures 13–15.

The percent ILF hiss occurrence for the noon sector shows reasonably strong AE* dependence. The other three MLT sectors show little or no difference in distribution from the annual AE distribution (black background).

For IHF hiss (not shown), Tsurutani et al. (2018) found AE* enhancements occurred not only in the noon sector but also in the dawn sector. This finding is in agreement with Malaspina et al. (2018) using a different set of data at different phases of the solar cycle.

Figure 13 gives the ILF plasmaspheric hiss event interval SYM-H* percent occurrence distributions for the four MLT sectors. From the upper left moving clockwise are the dawn, noon, midnight, and dusk sectors. Of the four MLT sectors, only the noon sector shows a prominent negative SYM-H* dependence. This same noon sector ILF hiss dependence was noted in Figure 12 for AE*.

Very few of the 10 ILF hiss intervals identified in the noon sector were associated with positive pressure SYM-H* values. This is in contrast to

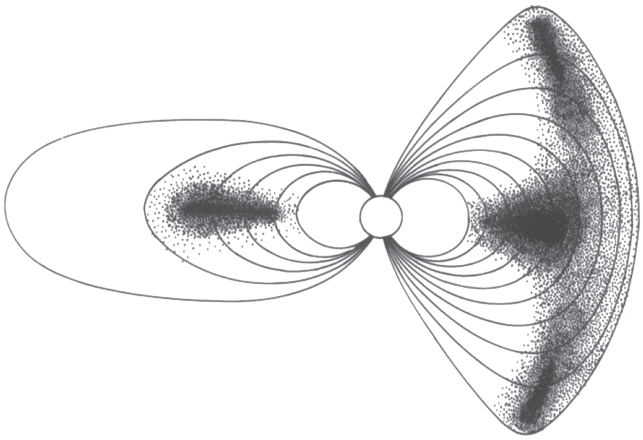

**Figure 16.** The Sun is on the right in the schematic. The solar wind compression of the outer region of the magnetosphere creates two "minimum B" pockets where the magnetic field is a local minimum in intensity. On the nightside, the minimum magnetic field strength is at the equator. The minimum magnetic field is also located at the equator on the dayside at low L. The dots represent chorus waves. Taken from Tsurutani and Smith (1977).

the general plasmaspheric hiss properties found by Falkowski et al. (2017). Since these SYM-H* > −50 nT, the geomagnetic activity by definition is not magnetic storms. The geomagnetic activity is most likely substorms/small convection events, such as HILDCAA intervals (Tsurutani et al., 2006).

In panel (c), the dusk sector shows both negative SYM-H* dependence and some positive SYM-H* dependence.

Previously, Tsurutani et al. (2018) noted IHF hiss-negative SYM-H* dependences for two MLT sectors, noon and dawn.

Figure 14 indicates the ram pressure of the solar wind during the ILF plasmaspheric hiss intervals. Panels (a) through (d) show the dawn, noon, dusk, and midnight sectors. The ILF plasmaspheric hiss is shown in the white bars as normalized percent occurrences. The ram pressure occurrence distribution over the year of study is shown in black in percent occurrence.

The most prominent result of all four local time sectors is that there appears to be no apparent dependence of ILF hiss intervals on high (or low) solar wind ram pressure. There may be a slight tendency for the midnight sector to be correlated with high pressures, but this is not a particularly strong feature.

The above result is in sharp contrast with IHF plasmaspheric hiss intervals. Tsurutani et al. (2018) showed that both the noon sector and midnight sector IHF hiss were strongly solar wind ram pressure dependent. The meaning of these differences will be discussed later in the paper. It is felt that this is a strong clue of the source of ILF plasmaspheric hiss.

## 4. Summary

The following are the main findings of our study of LF plasmaspheric hiss:

1. Using 1 year of ~22 Hz to ~200 Hz LF plasmaspheric hiss Polar search coil data taken during solar minimum (April 1996 to April 1997), it was found that LF plasmaspheric hiss was most intense in the noon-to-dusk local times (Figure 1). This is in general good agreement with Malaspina et al. (2018) and Meredith et al. (2018), surveys done in different phases of the solar cycle and with different spacecraft plasma wave data.
2. The ten most intense ~2 min 2 kHz bandwidth LF hiss events were selected from each of four local time sectors. For each one of these events, the data along the whole spacecraft track were collected to be able to study the entire event interval. It was found that there is no ILF hiss latitudinal |MLAT| dependence (Figure 11). The waves are equally intense from 0° to 50° |MLAT|. It should be mentioned that a lack of |MLAT| dependence of IHF hiss was also found by Tsurutani et al. (2018), in their Figure 11. Although these results are different than the two-peak |MLAT| distribution of both LF and HF hiss for average intensities at low L found by Meredith et al. (2018), it should be noted that the present survey focused on different LF hiss parameters than used by Meredith et al. (2018).
3. The 10 most intense ~2 min LF wave events were selected for each of four local time sectors. A packet of 5 wave cycles were selected from each of the 40 events, giving 200 individual cycles. From these 200 ILF wave cycles, it was found that ILF plasmaspheric hiss can be circularly, elliptically, or linearly/highly elliptically polarized (Figures 3–9), with most wave cycles determined to be elliptically polarized (Figure 9). Elliptical polarizations were detected for all $\theta_{kB}$ from 0° to 90°. It should be noted that hiss having elliptical polarizations is expected due to the high plasma densities within the plasmasphere (Verkhoglyadova et al., 2010).
4. The elliptically and linearly/highly elliptically polarized ILF plasmaspheric hiss had no obvious dependence on L and |MLAT| (Figures 7 and 8). The detection of ILF linearly polarized waves deep in the plasmasphere during relative geomagnetic quiet was a surprise (Figure 6). In this case there were many

packets of linearly polarized waves within the ~0.4 s interval. It is possible that the entire ~30 min intense wave event, encompassing not only ILF hiss but also IHF hiss, was linearly polarized. Thus it is possible that there is some relationship between plasmaspheric hiss and magnetosonic waves. There has been some speculation on this topic, but nothing has been done in detail to our knowledge.

5. The ILF hiss event interval percent occurrence dependences on AE* and SYM-H* were determined as a function of local time. ILF hiss was strongly AE* and SYM-H* dependent only in the noon sector (Figures 12 and 13). In contrast, IHF hiss were AE* and SYM-H* dependent for both the noon sector and the dawn sector (Tsurutani et al., 2018), indicating some differences between ILF and IHF hiss substorm dependences.
6. The solar wind ram pressure was studied for the ILF plasmaspheric hiss event interval data. There was no solar wind ram pressure ILF hiss dependence found in the noon sector (Figure 12). This result is in contrast to IHF hiss, where the noon (and midnight) sector intense waves had higher occurrence frequencies during high solar wind ram pressures.
7. ILF plasmaspheric hiss was found to be coherent for all MLT and |MLAT|. The waveforms and polarizations of ILF plasmaspheric hiss were quite similar to those of IHF plasmaspheric hiss. The above indicates several commonalities between ILF and IHF plasmaspheric hiss.
8. The 40 ILF plasmaspheric hiss events did not include data inside L = 3 or for L > ~7. LF hiss is definitely present in both of these regions (Figure 1), but not intense enough to make the cutoffs for the top ten events in each of the four local time sectors. Plasma plume (L > 7) LF and HF hiss were present, were coherent, and were intense (Falkowski et al., 2017; Tsurutani et al., 2015) but clearly less intense than the ILF/IHF hiss in the plasmasphere proper as shown here.

## 5. Discussion and Conclusions

Ten of the most intense ~2 min event data of LF plasmaspheric hiss were selected from each of the four local time sectors (covering all local times). All of the ILF hiss data examined contained coherent plasma waves. No segments of incoherent waves were found in this selected data set. Coherent wave interactions with cyclotron resonant electrons are approximately three orders of magnitude faster than incoherent wave-particle interactions. This has been shown previously in Tsurutani et al. (2009, & 2011), Lakhina et al. (2010), and Bellan (2013) and will not be repeated here for brevity. Thus, the presence of high intensity, coherent LF plasmaspheric hiss at all local times indicates that these waves, with the complement of IHF hiss, should dominate wave-particle interactions in the plasmasphere. It is highly likely that the L = 2 to 3 energetic electron slot/trough is formed by cyclotron interactions with these coherent waves during substorms/small injection events, particularly during solar wind high-speed stream HILDCAA intervals. These wave-particle interactions will take place not only at local noon (more intense in this local time sector because of the greater wave intensities) but also at all local times.

It should be mentioned that the obliquely propagating LF plasmaspheric hiss may have consequences other than just the precipitation for electrons in and near the slot region. Artemyev et al. (2012, 2015, 2016) have demonstrated that energetic electron interaction with such electromagnetic waves could lead to further particle energy gain, and Li et al. (2014) have shown that electron pitch angle scattering would be enhanced. Although this study was not conducted using solar maximum data, it also should be noted that inner zone plasmaspheric hiss is exceptionally intense during magnetic storms (Smith et al., 1974). Tsurutani et al. (1975) had previously noticed a LF hiss component at very low L during such events.

The ILF plasmaspheric hiss waves were found to be not only elliptically polarized, but some were circularly and linearly/highly elliptically polarized as well. Circularly polarized ILF hiss were detected more frequently with low $\theta_{kB}$ (parallel propagation) angles.

### 5.1. Interpretation of Results: A New Model

How can one interpret the present LF/ILF hiss findings? We will focus on the noon sector where LF hiss occurs most frequently and is most intense. In this paper, it was shown that in the noon sector, there was AE* and SYM-H* intense hiss dependences and a lack of solar wind ram pressure hiss dependence. IHF hiss in the noon sector also has substorm/injection event occurrence dependence. IHF hiss is composed of approximately three- to five-wave cycle coherent "packets" like ILF hiss. Thus from all of the similarities of IHF hiss with ILF hiss, it is quite likely that the origin of both waves is the same or quite similar.

In our previous paper on HF/IHF plasmaspheric hiss (Tsurutani et al., 2018), we proposed the idea that it was outer zone chorus which propagated from the outer magnetosphere to the plasmapause at low altitudes (high MLAT), entered the plasmasphere proper and then propagated and refracted throughout the plasmasphere. This follows the wave propagation ideas and raytracing results of Parrot et al. (2004), Bortnik et al. (2008), Bortnik, Thorne, and Meredith (2009), and Wang et al. (2011). In the Tsurutani et al., 2018 hypothesis, the authors went a step further and one coauthor (J.B.) performed wave ray tracing runs assuming that three different frequency chorus coherent "subelements" were all launched at the magnetic equator initially propagating parallel to the ambient magnetic field direction. This scenario is meant to investigate the further propagation of different frequency chorus subelements of a rising tone. The three subelements separated rapidly and enter the plasmasphere at different plasmapause locations. Thus as chorus subelements propagate away from their generation region, they separate and are no longer detected as rising tone elements. The various subelements separate from each other by diffractive effects. We believe that the ILF (and IHF) plasmaspheric hiss approximately three to five cycle packets are those chorus subelements. This was explained as a schematic shown in Figure 21 of Tsurutani et al. (2018) and is not repeated here for the sake of brevity.

What is special about local noon for chorus entering the plasmasphere? Won't the ~10 to 100 keV electron free energy be spent by the time they have gradient drifted from midnight, through dawn to local noon? It is clear that chorus wave generation occurs throughout this whole region (Meredith et al., 2001, 2012; Tsurutani & Smith, 1977) extracting the electron "free energy."

Figure 15 shows the presence of dayside high latitude chorus at |MLAT| > 30° taken from a past OGO-5 study. This distribution of chorus was attributed to solar wind compression of the dayside magnetosphere creating "minimum B pockets," regions of relatively low magnetic field magnitudes. Stated another way, the solar wind pressure creates a bifurcation of the magnetic equator where two regions of minimum magnetic field are both located away from the dipolar field position of the magnetic equator. One can think of this as two separate magnetic equators. Chorus is generated in regions where the magnetic field is a minimum. This is shown schematically in Figure 16.

Figure 16 illustrates chorus generation in the dayside minimum B pockets. These local magnetic field intensity minima are created by the solar wind compression of the dayside magnetosphere (the Sun is on the right). The minimum B pockets are a bifurcation of the normal dipole minimum magnetic fields at the equator and can appear at relatively high latitudes, particularly at noon where the compression effect is the greatest. The loss cone/temperature anisotropy instability has the greatest growth rate in these minimum B regions (Kennel & Petschek, 1966; Tsurutani & Lakhina, 1997).

Chorus generated in minimum B pockets will propagate away from the generation region in both directions. Thus waves propagating along the magnetic field toward the ionosphere will have a very short path length to reach the plasmapause and be refracted into the plasmasphere. Our argument is that this short path length minimizes Landau damping of the waves, allowing for greater intensity plasmaspheric hiss in the noon sector.

What is the source of the chorus? Our thought is that it is the ~10 to 100 keV electron cloud that is injected into the midnight sector of the magnetosphere during substorms and small injection events. As the cloud gradient drifts into the dayside magnetosphere, gradient drift effects will cause the perpendicular pitch angle particles to drift to greater L (called "drift shell splitting"), providing new free energy for instability and chorus growth. These "pancake" electron distribution functions will generate LF chorus very close to the dayside magnetopause (just before they are lost due to "magnetopause shadowing"; West et al., 1972), and the chorus subelements will propagate to the plasmapause and enter the plasmasphere.

The above scenario for ILF dayside intense plasmaspheric hiss can be easily tested. Using the Tsyganenko and Sitnov (2005) magnetospheric model and a wave raytracing code, one will be able to determine if such outer zone chorus can enter the plasmasphere and with what intensities. Particle detector and search coil magnetometer data can be used to determine if such unusual energetic electron pitch angles exist just inside the dayside magnetopause at high MLATs and if particularly LF chorus is generated. By "LF chorus," we are implying that chorus will be generated at a fraction of the electron cyclotron frequency, typically ~0.25 to 0.75 $\Omega_{CE}$ and sometimes less (Tsurutani & Smith, 1977). Because the Earth's magnetic fields are quite weak at the distant parts of the magnetosphere, this will be the

region where the minimum chorus wave frequencies will be generated. If these waves can propagate into the plasmasphere, they will become ILF hiss.

### 5.2. Midnight Sector Intense: Coherent Waves

Coherent ILF plasmaspheric hiss was detected in the midnight sector. However, surprisingly, this hiss was found to be not substorm dependent (Figure 12). The same lack of substorm dependence was also noted for IHF plasmaspheric hiss in the midnight sector (Tsurutani et al., 2018). What is an explanation? It is well known that midnight sector chorus is confined to regions close to the magnetic equator (Meredith et al., 2001; Tsurutani & Smith, 1974) because of strong wave Landau damping away from the equator. So midnight sector chorus generated during substorms will not be able to propagate to low altitudes to encounter the plasmapause and possibly gain entry into the plasmasphere.

Where does midnight sector hiss come from? One possibility is that it is dayside plasmaspheric hiss that has propagated to the nightside sector (Chen et al., 2009). 3-D wave raytracing code studies indicate that this is possible.

### 5.3. Final Comments

Inner zone (L < 6) relativistic electron cyclotron resonant interactions with the coherent and ILF plasmaspheric hiss could contribute to the loss of these particles during substorms. Because the plasma densities inside the plasmasphere are higher than outside, the electromagnetic wave phase speed will be considerably less within the plasmasphere than that in the lower-density outer region of the magnetosphere. The local magnetic field magnitudes will be considerably higher inside the plasmasphere due to the closer distances to Earth. Both of the above factors will lead to higher energies of electrons that will cyclotron resonate with the waves (Bortnik et al., 2011, Figure 2). The above hiss-energetic electron interaction mechanism will compete with anomalous cyclotron resonance between EMIC waves and high energy electrons. Calculations of the details of relativistic electron precipitation in the inner magnetosphere between these two plasma wave modes are beyond the scope of the present paper, but we encourage others to attempt to do this to determine the relative geoeffectiveness of the two wave modes. Are our results and interpretations in conflict with the Li et al. (2013) and Shi et al. (2017) mechanism of local generation of LF chorus (rising tone emissions) within the plasmasphere by in situ substorm ~100 keV electrons inside the plasmasphere? We think not. If the rising tone emissions are composed of coherent subelements, the different frequency subelements will disperse and will be detected throughout the plasmasphere as approximately three to five cycle coherent packets as shown in this paper. The question then becomes how much of LF hiss is due to which mechanism (outer magnetospheric chorus generation or internal plasmaspheric chorus generation) and are there other mechanisms also possible?

A coherent relatively large amplitude LF (and HF) hiss were detected in plasma plumes (L > 7). Hiss inside plumes have been reported previously (Shi et al., 2019; Summers et al., 2008; Teng et al., 2019; Tsurutani et al., 2015). We argue that because plumes are relatively small regions of space, the Thorne et al. (1979) mechanism of circulation of local plasmaspheric hiss with multiple passages through the generation region will not be applicable. Another approach to explain the observations would be to assume local generation by ~10 to 100 keV anisotropic electrons gradient drifting into the high-density plumes. However clearly quasi-linear theory/wave growth rates will not suffice. The fact that the hiss is coherent indicates the electron phase trapping is taking place perhaps making the wave growth rate substantially higher. This is a challenge for plasma wave theorists to come up with new models of instability/wave growth. As requested, we do the pitch angle diffusion calculations for both the incoherent and coherent waves. We use the example in Figure 4 where the density is 32/cm3 and Bo is 672 nT. At the request of one referee we have calculated the particle pitch angle transport and diffusion rates. We use the wave example in Figure 4. By hand measurements from the packet of 5 wave cycles occurring in a time duration of $\tau$=0.03 s. we find the wave frequency and the wave amplitude to be ~167 Hz and 0.1 nT, respectively. The measured background magnetic field intensity was B= 672 nT and electron number density, n= 32 $cm^{-3}$ at the L value of 6.9 and MLAT=40°. At this location there is no cyclotron resonant wave-particle interactions so these waves at this location are ineffective in scattering energetic electrons. However the waves are effective at other locations along the L = 6.9 magnetic field line. We do the calculation for the magnetic equator. We assume a dipole

magnetic field where the magnetic field strength along the field line varies with latitude, λ, as $B=B_0 (1+3 \sin^2\lambda)^{1/2} \cos^6\lambda$ (Tao et al., 2012) and an empirical model for the density variation with latitude along latitude λ on a magnetic field line as $n=n_0 \cos^{-4} \lambda$ (Denton et al., 2002). $B_0$ and $n_0$ denote the values at the equator. We find $B_0$ = 91 nT and $n_0$= 11 $cm^{-3}$. Considering the wave packet properties at equator to be the same as at MLAT=40°, we find the cyclotron resonant interaction is possible and get the Kennel-Petschek (incoherent wave) diffusion rate to be $D_{\alpha\alpha}$ =3.1×$10^{-3}$ $s^{-1}$, or a diffusion time tdiff = 325 s. Considering coherent waves, a single cyclotron resonant interaction of electron with the coherent wave packet can result in the pitch angle transport of 3.6° and a diffusion coefficient of D=0.28 $s^{-1}$ or a diffusion time of t=3.6 s. The diffusion due to coherent waves is two orders of magnitude faster than with incoherent waves.

More energetic electrons will be rapidly scattered by the coherent waves at off-axis locations. This is a different situation than for chorus where the off-axis chorus becomes incoherent (Tsurutani et al. 2013).

**Acknowledgments**
The Polar LF hiss plasma wave data can be obtained at CDAWeb (http://cdaweb.gsfc.nasa.gov). The solar wind time-shifted velocity and density data were obtained from the OMNI website (http://omniweb.gsfc.nasa.gov/). The solar wind ram pressure values were calculated from these data. The AE and SYM-H data used in this study was obtained from the WDC for Geomagnetism at Kyoto University (http://wdc.kugi.kyoto-u.ac.jp/wdc/Sec3.html). G.S.L is thankful to the Indian National Science Academy for the support under the INSA-Honorary Scientist Scheme. A.S. is thankful to the Indian National Science Academy (INSA) for the support under the INSA Senior Scientist Fellowship scheme. The work of R.H. is funded by the Science and Engineering Research Board (SERB), a statutory body of the Department of Science and Technology (DST), Government of India.

## References

Agapitov, O., Artemyev, A., Krasnoselskikh, V., Khotyaintsev, Y. V., Mourenas, D., Breuillard, H., et al. (2013). Statistics of whistler mode waves in the outer radiation belt: Cluster STAFF-SA measurements. *Journal of Geophysical Research: Space Physics*, *118*, 3407–3420. https://doi.org/10.1002/jgra.50312

Agapitov, O. V., Artemyev, A. V., Mourenas, D., Kasahara, Y., & Krasnoselskikh, V. (2014). Inner belt and slot region electron lifetimes and energization rates based on Akebono statistics of whistler waves. *Journal of Geophysical Research: Space Physics*, *119*, 2876–2893. https://doi.org/10.1002/2014JA019886

Agapitov, O. V., Mourenas, D., Artemyev, A., Mozer, F. S., Bonnell, J. W., Angelopoulos, V., et al. (2018). Spatial extent and temporal correlation of chorus and hiss: Statistical results from multi-point THEMIS observations. *Journal of Geophysical Research: Space Physics*, *123*, 8317–8330. https://doi.org/10.1029/2018JA025725

Artemyev, A., Agapitov, O., Breuillard, H., Krasnoselskikh, V., & Rolland, G. (2012). Electron pitch-angle diffusion in radiation belts: The effects of whistler wave oblique propagation.*Geophysical Research Letters*, *39*, L08105. https://doi.org/10.1029/2012GL051393

Artemyev, A., Agapitov, O., Mourenas, D., Krasnoselskikh, V., Shastun, V., & Mozer, F. (2016). Oblique whistler-mode waves in the Earth's inner magnetosphere: Energy distribution, origins, and role in radiation belt dynamics. *Space Science Reviews*, *200*(1-4), 261–355. https://doi.org/10.1007/s11214-016-0252-5

Artemyev, A. V., Agapitov, O. V., Mourenas, D., Krasnoselskikh, V. V., & Mozer, F. S. (2015). Wave energy budget analysis in the Earth's radiation belts uncovers a missing energy. *Nature Communications*, *6*(1). https://doi.org/10.1038/ncomms8143

Bellan, P. M. (2013). Pitch angle scattering of an energetic magnetized particle by a circularly polarized electromagnetic wave. *Physics of Plasmas*, *20*(4), 042117. https://doi.org/10.1063/1.4801055

Bortnik, J., Chen, L., Li, W., Thorne, R. M., Meredith, N. P., & Horne, R. B. (2011). Modeling the wave power distribution and characteristics of plasmaspheric hiss. *Journal of Geophysical Research*, *116*, A12209. https://doi.org/10.1029/2011JA016862

Bortnik, J., Li, W., Thorne, R. M., Angelopoulos, V., Cully, C., Bonnell, J., et al. (2009). An observation linking the origin of plasmaspheric hiss to discrete chorus emissions. *Science*, *324*(5928), 775–778. https://doi.org/10.1126/science.1171273

Bortnik, J., Thorne, R. M., & Meredith, N. P. (2008). The unexpected origin of plasmaspheric hiss from discrete chorus emissions. *Nature*, *452*(7183), 62–66. https://doi.org/10.1038/nature06741

Bortnik, J., Thorne, R. M., & Meredith, N. P. (2009). Plasmaspheric hiss overview and relation to chorus. *Journal of Atmospheric and Solar - Terrestrial Physics*, *71*(16), 1636–1646. https://doi.org/10.1016/j.jastp.2009.03.023

Breneman, A. W., Kletzing, C. A., Pickett, J., Chum, J., & Santolik, O. (2009). Statistics of multispacecraft observations of chorus dispersion and source location. *Journal of Geophysical Research*, *114*, A06202. https://doi.org/10.1029/2008JA013549

Carpenter, D. L. (1978). New whistler evidence of a dynamo origin of electric fields in the quiet plasma. *Journal of Geophysical Research*, *83*, 44.

Cattell, C., Breneman, A. W., Thaller, S. A., Wygant, J. R., Kletzing, C. A., & Kurth, W. S. (2015). Van Allen Probes observations of unusually low frequency whistler mode waves observed in association with moderate magnetic storms: Statistical study. *Geophysical Research Letters*, *42*, 7273–7281. https://doi.org/10.1002/2015GL065565

Chen, A. J., & Grebowsky, J. M. (1974). Plasma tail interpretations of pronounced detached plasma regions measured by OGO 5. *Journal of Geophysical Research*, *79*(25), 3851–3855. https://doi.org/10.1029/JA079i025p03851

Chen, L., Bortnik, J., Li, W., Thorne, R. M., & Horne, R. B. (2012). Modeling the properties of plasmaspheric hiss: 1. Dependence on chorus wave emission. *Journal of Geophysical Research*, *117*, A05201. https://doi.org/10.1029/2011JA017201

Chen, L., Bortnik, J., Thorne, R. M., Horne, R. B., & Jordanova, V. K. (2009). Three-dimensional ray tracing of VLF waves in a magnetospheric environment containing a plasma plume. *Geophysical Research Letters*, *36*, L22101. https://doi.org/10.1029/2009GL040451

Chen, L., Thorne, R. M., Bortnik, J., Li, W., Horne, R. B., Reeves, G. D., et al. (2014). Generation of unusually low frequency plasmaspheric hiss. *Geophysical Research Letters*, *41*, 5702–5709. https://doi.org/10.1002/2014GL060628

Cornilleau-Wehrlin, N., Gendrin, R., Lefeuvre, F., Parrot, M., Grard, R., Jones, D., et al. (1978). VLF electromagnetic waves observed onboard GEOS-1. *Space Science Reviews*, *22*, 371.

Cornilleau-Wehrlin, N., Solomon, J., Korth, A., & Kremser, G. (1993). Generation mechanism of plasmaspheric ELF/VLF hiss: A statistical study from GEOS 1 data. *Journal of Geophysical Research*, *98*(A12), 21,471–21,479. https://doi.org/10.1029/93JA01919

Delport, B., Collier, A. B., Lichtenberger, J., Rodger, C. J., Parrot, M., Clilverd, M. A., & Friedel, R. H. W. (2012). Simultaneous observation of chorus and hiss near the plasmapause. *Journal of Geophysical Research*, *117*, A12218. https://doi.org/10.1029/2012JA017609

Denton, R. E., Goldstein, J., & Menietti, J.D. (2002). Field line dependence of magnetospheric electron density. *Geophys. Res. Lett.*, *2205*, https://doi.org/10.1029/2012GL051202.

Dragonov, A. B., Inan, U. S., Sonwalkar, V. S., & Bell, T. F. (1992). Magnetospherically reflected whistlers as a source of plasmaspheric hiss. *Geophysical Research Letters*, *19*(3), 233–236. https://doi.org/10.1029/91GL03167

Echer, E., Gonzalez, W. D., Tsurutani, B. T., & Gonzalez, A. L. C. (2008). Interplanetary conditions causing intense geomagnetic storms (Dst < -100 nT) during solar cycle 23 (1996-2006). *Journal of Geophysical Research*, *113*, A05221. https://doi.org/10.1029/2007JA012744

Falkowski, B. J., Tsurutani, B. T., Lakhina, G. S., & Pickett, J. S. (2017). Two sources of dayside intense, quasi-coherent plasmaspheric hiss: A new mechanism for the slot region? *Journal of Geophysical Research: Space Physics*, *122*, 1643–1657. https://doi.org/10.1002/2016JA023289

Gail, W. B., & Inan, U. S. (1990). Characteristics of wave-particle interactions during sudden commencements: 2. Spacecraft observations. *Journal of Geophysical Research*, *95*(A1), 139–147. https://doi.org/10.1029/JA095iA01p00139

Gao, Y., Xiao, F., Yan, Q., Yang, C., Liu, S., He, Y., & Zhou, Q. (2015). Influence of wave normal angles on hiss-electron interactions in Earth's slot region. *Journal of Geophysical Research: Space Physics*, *120*, 9385–9400. https://doi.org/10.1002/2015JA021786

Gao, Z., Su, Z., Xiao, F., Zheng, H., Wang, Y., Wang, S., et al. (2018). Exohiss wave enhancement following substorm electron injection in the dayside magnetosphere. *Earth and Planetary Physics*, *2*, 359–370. https://doi.org/10.26464/epp2018033

Glauert, S. A., Horne, R. B., & Meredith, N. P. (2014). Three-dimensional electron radiation belt simulations using the BAS radiation belt model with new diffusion models for chorus, plasmaspheric hiss and lightning-generated whistlers. *Journal of Geophysical Research: Space Physics*, *119*, 268–289. https://doi.org/10.1002/2013JA019281

Gonzalez, W. D., Joselyn, J. A., Kamide, Y., Kroehl, H. W., Rostoker, G., Tsurutani, B. T., & Vasyliunas, V. M. (1994). What is a geomagnetic storm? *Journal of Geophysical Research*, *99*(A4), 5771. https://doi.org/10.1029/93JA02867

Green, J. L., Boardsen, S., Garcia, L., Taylor, W. W. L., Fung, S. F., & Reinisch, B. W. (2005). On the origin of whistler mode radiation in the plasmasphere. *Journal of Geophysical Research*, *110*, A03201. https://doi.org/10.1029/2004JA010495

Gurnett, D. A., Persoon, A. M., Randall, R. F., Odem, D. L., Remington, S. L., Averkamp, T. F., et al. (1995). The Polar plasma wave instrument. *Space Science Reviews*, *71*(1-4), 597–622. https://doi.org/10.1007/BF00751343

Hajra, R., Echer, E., Tsurutani, B. T., & Gonzalez, W. D. (2013). Solar cycle dependence of high-intensity long-duration continuous AE activity (HILDCAA) events, relativistic electron predictors? *Journal of Geophysical Research: Space Physics*, *118*, 5626–5638. https://doi.org/10.1002/jgra.50530

Hajra, R., Echer, E., Tsurutani, B. T., & Gonzalez, W. D. (2014). Superposed epoch analyses of HILDCAAs and their interplanetary drivers: Solar cycle and seasonal dependences. *Journal of Atmospheric and Solar - Terrestrial Physics*, *121*, 24–31. https://doi.org/10.1016/j.jastp.2014.09.012

Hartley, D. P., Kletzing, C. A., Chen, L., Horne, R. B., & Santolik, O. (2019). Van Allen Probes observations of chorus wave vector orientations: Implications for the chorus-to-hiss mechanism. *Geophysical Research Letters*, *46*, 2337–2346. https://doi.org/10.1029/2019GL082111

Hartley, D. P., Kletzing, C. A., Santolik, O., Chen, L., & Horne, R. B. (2018). Statistical properties of plasmaspheric hiss from Van Allen Probes observations. *Journal of Geophysical Research: Space Physics*, *123*, 2605–2619. https://doi.org/10.1002/2017JA024593

He, Z., Chen, L., Liu, X., Zhu, H., Liu, S., Gao, Z., & Cao, Y. (2019). Local generation of high-frequency plasmaspheric hiss observed by Van Allen Probes. *Geophysical Research Letters*, *46*, 1141–1148. https://doi.org/10.1029/2018GL081578

Hua, M., Ni, B., Li, W., Gu, X., Fu, S., Shi, R., et al. (2019). Evolution of radiation belt electron pitch angle distribution due to combined scattering by plasmaspheric hiss and magnetosonic waves. *Geophysical Research Letters*, *46*, 3033–3042. https://doi.org/10.1029/2018GL081828

Kavanagh, A. J., Cobbett, N., & Kirsch, P. (2018). Radiation belt slot-region filling events: Sustained energetic precipitation into the mesosphere. *Journal of Geophysical Research: Space Physics*, *123*, 7999–8020. https://doi.org/10.1029/2018JA025890

Kennel, C. F., & Petschek, H. E. (1966). Limits on stably trapped particle fluxes. *Journal of Geophysical Research*, *71*(1), 1–28. https://doi.org/10.1029/JZ071i001p00001

Kim, K.-C., Lee, D.-Y., & Shprits, Y. (2015). Dependence of plasmaspheric hiss on solar wind parameters and geomagnetic activity and modeling of its global distribution. *Journal of Geophysical Research: Space Physics*, *120*, 1153–1167. https://doi.org/10.1002/2014JA020687

Kim, K.-C., & Shprits, Y. (2019). Statistical analysis of hiss waves in plasmaspheric plumes using Van Allen Probe observations. *Journal of Geophysical Research: Space Physics*, *124*, 1904–1915. https://doi.org/10.1029/2018JA026458

Kokubun, S. (1983). Characteristics of storm sudden commencements at geostationary orbit. *Journal of Geophysical Research*, *88*(A12), 10,025. https://doi.org/10.1029/JA088iA12p10025

Lakhina, G. S., Tsurutani, B. T., Verkhoglyadova, O. P., & Pickett, J. S. (2010). Pitch angle transport of electrons due to cyclotron interactions with coherent chorus subelements. *Journal of Geophysical Research*, *117*, A00F15. https://doi.org/10.1029/2009JA014885

Li, W., Chen, L., Bortnik, J., Thorne, R. M., Angelopoulos, V., Kletzing, C. A., et al. (2015). First evidence for chorus at a large geocentric distance as a source of plasmaspheric hiss: Coordinated THEMIS and Van Allen Probes observation. *Geophysical Research Letters*, *42*, 241–248. https://doi.org/10.1002/2014GL062832

Li, W., Chen, L., Bortnik, J., Thorne, R. M., Angelopoulos, V., Kletzing, C. A., et al. (2017). First evidence for chorus at a large geocentric distance as a source of plasmaspheric hiss: Coordinated THEMIS and Van Allen Probes observation. *Geophysical Research Letters*, *42*, 241–248. https://doi.org/10.1002/2014GL062832

Li, W., Ma, Q., Thorne, R. M., Bortnik, J., Kletzing, C. A., Kurth, W. S., et al. (2015). Statistical properties of plasmaspheric hiss derived from Van Allen Probes data and their effects on radiation belt electron dynamics. *Journal of Geophysical Research: Space Physics*, *120*, 3393–3405. https://doi.org/10.1002/2015JA021048

Li, W., Mourenas, D., Artemyev, A. V., Agapitov, O. V., Bortnik, J., Albert, J. M., et al. (2014). Evidence of stronger pitch angle scattering loss caused by oblique whistler-mode waves as compared with quasi-parallel waves. *Geophysical Research Letters*, *41*, 6063–6070. https://doi.org/10.1002/2014GL061260

Li, W., Shen, X.-C., Ma, Q., Capannolo, L., Shi, R., Redmon, R. J., et al. (2019). Quantification of energetic electron precipitation driven by plume whistler mode waves, plasmaspheric hiss and exohiss. *Geophysical Research Letters*, *46*, 3615–3624. https://doi.org/10.1029/2019GL082095

Li, W., Thorne, R. M., Bortnik, J., Reeves, G. D., Kletzing, C. A., Kurth, W. S., et al. (2013). An unusual enhancement of low-frequency plasmaspheric hiss in the outer plasmasphere associated with substorm-injected electrons. *Geophysical Research Letters*, *40*, 3798–3803. https://doi.org/10.1002/grl.50787

Malaspina, D. M., Jaynes, A. N., Boule, C., Bortnik, J., Thaller, S. A., Ergun, R. E., et al. (2016). The distribution of plasmaspheric hiss wave power with respect to the plasmapause location. *Geophysical Research Letters*, *43*, 7878–7886. https://doi.org/10.1002/2016GL069982

Malaspina, D. M., Jaynes, A. N., Hospodarsky, G., Bortnik, J., Ergun, R. E., & Wygant, J. (2017). Statistical properties of low-frequency plasmaspheric hiss. *Journal of Geophysical Research: Space Physics*, *122*, 8340–8352. https://doi.org/10.1002/2017JA024328

Malaspina, D. M., Ripoll, J.-F., Chu, X., Hospodarsky, G., & Wygant, J. (2018). Variation in plasmaspheric hiss wave power with plasma density. *Geophysical Research Letters*, *45*, 9417–9426. https://doi.org/10.1029/2018GL078564

Meredith, N. P., Horne, R. B., & Anderson, R. R. (2001). Substorm dependence of chorus amplitudes: Implications for the acceleration of electrons to relativistic energies. *Journal of Geophysical Research*, *106*(A7), 13,165–13,178. https://doi.org/10.1029/2000JA900156

Meredith, N. P., Horne, R. B., Clilverd, M. A., Horsfall, D., Thorne, R. M., & Anderson, R. R. (2006). Origins of plasmaspheric hiss. *Journal of Geophysical Research*, *111*, A09217. https://doi.org/10.1029/2006JA011707

Meredith, N. P., Horne, R. B., Glauert, S. A., & Anderson, R. R. (2007). Slot region electron loss timescales due to plasmaspheric hiss and lightning-generated whistlers. *Journal of Geophysical Research*, *112*, A08214. https://doi.org/10.1029/2007JA012413

Meredith, N. P., Horne, R. B., Kersten, T., Li, W., Bortnik, J., Sicard, A., & Yearby, K. H. (2018). Global model of plasmaspheric hiss from multiple satellite observations. *Journal of Geophysical Research: Space Physics*, *123*, 4526–4541. https://doi.org/10.1029/2018JA025226

Meredith, N. P., Horne, R. B., Sicard-Piet, A., Boscher, D., Yearby, H., Li, W., & Thorne, R. M. (2012). Global model of lower band and upper band chorus from multiple satellite observations. *Journal of Geophysical Research*, *117*, A10225. https://doi.org/10.1029/2012JA017978

Meredith, N. P., Horne, R. B., Thorne, R. M., Summers, D., & Anderson, R. R. (2004). Substorm dependence of plasmaspheric hiss. *Journal of Geophysical Research*, *109*, A06209. https://doi.org/10.1029/2004JA010387

Nakamura, S., Omura, Y., & Summers, D. (2018). Fine structure of whistler-mode hiss in plasmaspheric plumes observed by the Van Allen Probes. *Journal of Geophysical Research: Space Physics*, *123*, 9055–9064. https://doi.org/10.1029/2018JA025803

Ni, B., Hua, M., Zhou, R., Yi, J., & Fu, S. (2017). Competition between outer zone electron scattering by plasmaspheric hiss and magnetosonic waves. *Geophysical Research Letters*, *44*, 3465–3474. https://doi.org/10.1002/2017GL072989

Ni, B., Huang, H., Zhang, W., Gu, X., Zhao, H., Li, X., et al. (2019). Parametric sensitivity of the formation of reversed electron energy spectrum caused by plasmaspheric hiss. *Geophysical Research Letters*, *46*(8), 4134–4143. https://doi.org/10.1029/2019GL082032

Parrot, M., Santolik, O., Gurnett, D., Pickett, J., & Cornilleau-Wehrlin, N. (2004). Characteristics of magnetospherically reflected chorus waves observed by Cluster. *Annales de Geophysique*, *22*(7), 2597–2606. https://doi.org/10.5194/angeo-22-2597-2004

Russell, C. T., Holzer, R. E., & Smith, E. J. (1969). OGO 3 observations of ELF noise in the magnetosphere: 1. Spatial extent and frequency of occurrence. *Journal of Geophysical Research*, *74*(3), 755–777. https://doi.org/10.1029/JA074i003p00755

Santolik, O. (2008). New results of investigations of whistler-mode chorus emissions. *Nonlinear Processes in Geophysics*, *15*(4), 621–630. https://doi.org/10.5194/npg-15-621-2008

Santolik, O., & Chum, J. (2009). The origin of plasmaspheric hiss. *Science*, *324*(5928), 729–730. https://doi.org/10.1126/science.1172878

Santolik, O., Chum, J., Parrot, M., Gurnett, D. A., Pickett, J. S., & Cornilleau-Wehrlin, N. (2006). Propagation of whistler mode chorus to low altitudes: Spacecraft observations of structured ELF hiss. *Journal of Geophysical Research*, *111*, A10208. https://doi.org/10.1029/2005JA011462

Santolik, O., Parrot, M., Storey, L. R. O., Pickett, J. S., & Gurnett, D. A. (2001). Propagation analysis of plasmaspheric hiss using Polar PWI measurements. *Geophysical Research Letters*, *28*(6), 1127–1130. https://doi.org/10.1029/2000GL012239

Santolik, O., Pickett, J. S., Gurnett, D. A., Maksimovic, M., & Cornilleau-Wehrlin, N. (2002). Spatiotemporal variability and propagation of equatorial noise observed by Cluster. *Journal of Geophysical Research*, *107*(A12), 1495. https://doi.org/10.1029/2001JA009159

Shi, R., Li, W., Ma, Q., Claudepierre, S. G., Kletzing, C. A., Kurth, W. S., et al. (2018). Van Allen Probes observation of plasmaspheric hiss modulated by injected energetic electrons. *Annali di Geofisica*, *36*(3), 781–791. https://doi.org/10.5194/angeo-36-781-2018

Shi, R., Li, W., Ma, Q., Green, A., Kletzing, C. A., Kurth, W. S., et al. (2019). Properties of whistler mode waves in Earths plasmasphere and plumes. *Journal of Geophysical Research: Space Physics*, *124*, 1035–1051. https://doi.org/10.1029/2018JA026041

Shi, R., Li, W., Ma, Q., Reeves, G. D., Kletzing, C. A., Kurth, W. S., et al. (2017). Systematic evaluation of low-frequency hiss and energetic electron injections. *Journal of Geophysical Research: Space Physics*, *122*, 10,263–10,274. https://doi.org/10.1002/2017JA024571

Shinbori, A., Ono, T., Iizima, M., & Kumamoto, A. (2003). Sudden commencements related plasma waves observed by the Akebono satellite in the polar region and inside the plasmasphere region. *Journal of Geophysical Research*, *108*(A12), 1457. https://doi.org/10.1029/2003JA009964

Smith, E. J., Frandsen, A. M. A., Tsurutani, B. T., Thorne, R. M., & Chan, K. W. (1974). Plasmasheric hiss intensity variations during magnetic storms. *Journal of Geophysical Research*, *79*(16), 2507–2510. https://doi.org/10.1029/JA079i016p02507

Smith, E. J., & Tsurutani, B. T. (1976). Magnetosheath lion roars. *Journal of Geophysical Research*, *81*(13), 2261–2266. https://doi.org/10.1029/JA081i013p02261

Smith, E. J., & Wolfe, J. H. (1976). Observations of interaction regions and corotating shocks between one and five AU: Pioneers 10 and 11. *Geophysical Research Letters*, *3*(3), 137–140. https://doi.org/10.1029/GL003i003p00137

Solomon, J., Cornilleau-Wehrlin, N., Korth, A., & Kremser, G. (1988). An experimental study of ELF/VLF hiss generation in the Earth's magnetosphere. *Journal of Geophysical Research*, *93*(A3), 1839. https://doi.org/10.1029/JA093iA03p01839

Sonwalkar, V. S., & Inan, U. S. (1989). Lightning as an embryonic source of VLF hiss. *Journal of Geophysical Research*, *94*(A6), 6986–6994. https://doi.org/10.1029/JA094iA06p06986

Spasojevic, M., Shprits, Y. Y., & Orlova, K. (2015). Global empirical models of plasmaspheric hiss using Van Allen probes. *Journal of Geophysical Research: Space Physics*, *120*, 10,370–10,383. https://doi.org/10.1002/2015JA021803

Storey, L. R. O., Lefeuvre, F., Parrot, M., Cairo, L., & Anderson, R. R. (1991). Initial survey of the wave distribution functions for plasmaspheric hiss observed by ISEE-1. *Journal of Geophysical Research*, *96*(A11), 19,469. https://doi.org/10.1029/91JA01828

Su, Z., Liu, N., Zheng, H., Wang, Y., & Wang, S. (2018). Multipoint observations of nightside plasmaspheric hiss generated by substorm-injected electrons. *Geophysical Research Letters*, *45*, 10,921–10,932. https://doi.org/10.1029/2018GL079927

Summers, D., Ni, B., Meredith, N. P., Horne, R. B., Thorne, R. M., Moldwin, M. B., & Anderson, R. R. (2008). Electron scattering by whistler-mode ELF hiss in plasmaspheric plumes. *Journal of Geophysical Research*, *113*, A04219. https://doi.org/10.1029/2007JA012678

Summers, D., Omura, Y., Nakamura, S., & Kletzing, C. A. (2014). Fine structure of plasmaspheric hiss. *Journal of Geophysical Research: Space Physics*, *119*, 9134–9149. https://doi.org/10.1002/2014JA020437

Tao, X., Bortnik, R. M., Thorne, R.M., Albert, J.M., & Li, W. (2012). Effects of amplitude modulation on nonlinear interactions between electrons and chorus waves. *Geophys. Res. Lett.*, *39*, L06102 doi:10.1029/2012GL051202.

Teng, S., Li, W., Tao, X., Shen, X.-C., & Ma, Q. (2019). Characteristics of rising tone whistler mode waves inside the Earth's plasmasphere, plasmaspheric plumes and plasmatrough. *Geophysical Research Letters*, *46*, 7121–7130. https://doi.org/10.1029/2019GL083372

Thorne, R. M. (2010). Radiation belt dynamics: The importance of wave-particle interactions. *Geophysical Research Letters*, *37*, L22107. https://doi.org/10.1029/2010GL044990

Thorne, R. M., Church, S. R., & Gorney, D. J. (1979). On the origin of plasmaspheric hiss: The importance of wave propagation during periods of substorm activity. *Journal of Geophysical Research*, *84*(A9), 5241. https://doi.org/10.1029/JA084iA09p05241

Thorne, R. M., Church, S. R., Malloy, W. J., & Tsurutani, B. T. (1977). The local time variation of ELF emissions during periods of substorm activity. *Journal of Geophysical Research*, *82*(10), 1585–1590. https://doi.org/10.1029/JA082i010p01585

Thorne, R. M., Smith, E. J., Burton, R. K., & Holzer, R. E. (1973). Plasmaspheric hiss. *Journal of Geophysical Research*, *78*(10), 1581–1596. https://doi.org/10.1029/JA078i010p01581

Tsurutani, B. T., Falkowski, B. J., Pickett, J. S., Santolik, O., & Lakhina, G. S. (2015). Plasmaspheric hiss properties: Observations from Polar. *Journal of Geophysical Research: Space Physics*, *120*, 414–431. https://doi.org/10.1002/2014JA020518

Tsurutani, B. T., Falkowski, B. J., Pickett, J. S., Verkhoglyadova, O. P., Santolik, O., & Lakhina, G. S. (2014). Extremely intense ELF magnetosonic waves: A survey of Polar observations. *Journal of Geophysical Research: Space Physics*, *119*, 964–977. https://doi.org/10.1002/2013JA019284

Tsurutani, B. T., Falkowski, B. J., Verkhoglyadova, O. P., Pickett, J. S., Santolik, O., & Lakhina, G. S. (2011). Quasi-coherent chorus properties: 1. Implications for wave-particle interactions. *Journal of Geophysical Research*, *116*, A09210. https://doi.org/10.1029/2010JA016237

Tsurutani, B. T., Falkowski, B. J., Verkhoglyadova, O. P., Pickett, J. S., Santolik, O., & Lakhina, G. S. (2012). Dayside ELF electromagnetic wave survey: A Polar statistical study of chorus and hiss. *Journal of Geophysical Research*, *117*, A00L12. https://doi.org/10.1029/2011JA017180

Tsurutani, B. T., & Gonzalez, W. D. (1987). The cause of high-intensity long-duration continuous AE activity (HILDCAAS): Interplanetary Alfven wave trains. *Planetary and Space Science*, *35*(4), 405–412. https://doi.org/10.1016/0032-0633(87)90097-3

Tsurutani, B. T., Gonzalez, W. D., Gonzalez, A. L. C., Guarnieri, F. L., Gopalswamy, N., Grande, M., et al. (2006). Corotating solar wind streams and recurrent geomagnetic activity: A review. *Journal of Geophysical Research*, *111*, A07S01. https://doi.org/10.1029/2005JA011273

Tsurutani, B. T., Gonzalez, W. D., Gonzalez, A. L. C., Tang, F., Arballo, J. K., & Okada, M. (1995). Interplanetary origin of geomagnetic activity in the declining phase of the solar cycle. *Journal of Geophysical Research*, *100*(A11), 21,717–21,733. https://doi.org/10.1029/95JA01476

Tsurutani, B. T., Gonzalez, W. D., Guarnieri, F., Kamide, Y., Zhou, X.-Y., & Arballo, J. K. (2004). Are high-intensity, long-duration continuous AE activity (HILDCAA) events substorm expansion events? *Journal of Atmospheric and Solar - Terrestrial Physics*, *66*(2), 167–176. https://doi.org/10.1016/j.jastp.2003.08.015

Tsurutani, B. T., Gonzalez, W. D., Tang, F., Akasofu, S. I., & Smith, E. J. (1988). Origin of interplanetary southward magnetic fields responsible for major magnetic storms near solar maximum (1978-1979). *Journal of Geophysical Research*, *93*(A8), 8519–8531. https://doi.org/10.1029/JA093iA08p08519

Tsurutani, B. T., & Lakhina, G. S. (1997). Some basic concepts of wave-particle interactions in collisionless plasmas. *Reviews of Geophysics*, *35*(4), 491–501. https://doi.org/10.1029/97RG02200

Tsurutani, B. T., Lakhina, G. S., & Verkhoglyadova, O. P. (2013). Energetic electron (> 10 keV) microburst precipitation, ~5−15 s X-ray pulsations, chorus, and wave-particle interactions: A review. *J. Geophys. Res. Spa. Phys.*, *118*, doi:10.1002/jgra.50264.

Tsurutani, B. T., Park, S. A., Falkowski, B. J., Lakhina, G. S., Pickett, J. S., Bortnik, J., et al. (2018). Plasmaspheric hiss: Coherent and intense. *Journal of Geophysical Research: Space Physics*, *123*, 10,009–10,029. https://doi.org/10.1029/2018JA025975

Tsurutani, B. T., & Smith, E. J. (1974). Postmidnight chorus: A substorm phenomenon. *Journal of Geophysical Research*, *79*(1), 118–127. https://doi.org/10.1029/JA079i001p00118

Tsurutani, B. T., & Smith, E. J. (1977). Two types of magnetospheric ELF chorus and their substorm dependences. *Journal of Geophysical Research*, *82*(32), 5112–5128. https://doi.org/10.1029/JA082i032p05112

Tsurutani, B. T., Smith, E. J., & Thorne, R. M. (1975). Electromagnetic hiss and relativistic electron losses in the inner zone. *Journal of Geophysical Research*, *80*(4), 600–607. https://doi.org/10.1029/JA080i004p00600

Tsurutani, B. T., Smith, E. J., West, H. I. Jr., & Buck, R. M. (1979). Chorus, energetic electrons and magnetospheric substorms. In P. J. Palmadesso & K. Papadopoulos (Eds.), *Wave instabilities in space plasmas* (pp. 55–72). Washington, DC: D. Reidel Publ. Co.

Tsurutani, B. T., Verkhoglyadova, O. P., Lakhina, G. S., & Yagitani, S. (2009). Properties of dayside outer zone chorus during HILDCAA events: Loss of energetic electrons. *Journal of Geophysical Research*, *114*, A03207. https://doi.org/10.1029/2008JA013353

Tsyganenko, N. A., & Sitnov, M. I. (2005). Modeling the dynamics of the inner magnetosphere during strong geomagnetic storms. *Journal of Geophysical Research*, *110*, A03208. https://doi.org/10.1029/2004JA010798

Verkhoglyadova, O. P., Tsurutani, B. T., & Lakhina, G. S. (2010). Properties of obliquely propagating chorus. *Journal of Geophysical Research*, *115*, A00F19. https://doi.org/10.1029/2009JA014809

Wang, C., Zong, Q., Xiao, F., Su, Z., Wang, Y., & Yue, C. (2011). The relations between magnetospheric chorus and hiss inside and outside the plasmasphere boundary layer: Cluster observation. *Journal of Geophysical Research*, *116*, A07221. https://doi.org/10.1029/2010JA016240

West, H. I. Jr., Buck, R. M., & Walton, J. R. (1972). Shadowing of electron azimuthal-drift motions near the noon magnetopause. *Nature Physical Sciences*, *240*(97), 6–7. https://doi.org/10.1038/physci240006a0

Yu, J., Li, L. Y., Cao, J. B., Chen, L., Wang, J., & Yang, J. (2017). Propagation characteristics of plasmaspheric hiss: Van Allen Probe observations and global empirical models. *Journal of Geophysical Research: Space Physics*, *122*, 4156–4167. https://doi.org/10.1002/2016JA023372

Zahlava, J., Nemec, F., Santolik, O., Kolmasova, I., Hospodarsky, G. B., Parrot, M., et al. (2018). Longitudinal dependence of whistler mode electromagnetic waves in the Earth's inner magnetosphere. *Journal of Geophysical Research: Space Physics*, *123*, 6562–6575. https://doi.org/10.1029/2018JA025284

Zhang, W., Fu, S., Gu, X., Ni, B., Xiang, Z., Summers, D., et al. (2018). Electron scattering by plasmaspheric hiss in a nightside plume. *Geophysical Research Letters*, *45*, 4618–4627. https://doi.org/10.1029/2018GL077212

Zhao, H., Ni, B., Li, X., Baker, D. N., Johnston, W. R., Zhang, W., et al. (2019). Plasmaspheric hiss waves generate a reversed energy spectrum of radiation belt electrons. *Nature Physics Letters*, *15*(4), 367–372. https://doi.org/10.1038/s41567-018-0391-6